

TPR-96-12; HZPP-96-7;

Yano-Koonin-Podgoretskii Parametrisation of the HBT Correlator: A Numerical Study

Wu Y.-F.^{1,*}, U. Heinz^{1,2}, B. Tomášik¹, and U.A. Wiedemann¹¹*Institut für Theoretische Physik, Universität Regensburg,**D-93040 Regensburg, Germany*²*CERN/TH, CH-1211 Geneva 23, Switzerland*

(December 2, 2024)

Abstract

The Yano-Koonin-Podgoretskii (YKP) parametrisation of Hanbury-Brown/Twiss (HBT) two-particle correlation functions opens new strategies for extracting the emission duration and testing the longitudinal expansion in heavy-ion collisions. Based on the recently derived model-independent expressions, we present a detailed parameter study of the YKP fit parameters for a hydrodynamic finite expanding source model of heavy-ion collisions. Our study supports the clean spatio-temporal interpretation of the three YKP radius parameters as longitudinal extension, transverse extension and emission duration of the source in the YKP Lorentz frame. This frame is specified by the fourth fit parameter, the Yano-Koonin velocity which describes to a good approximation the velocity of the fluid element with highest emissivity and allows to test for the longitudinal expansion of the source. Deviations from this interpretation of the YKP parameters are quantitatively discussed and found to be generically small.

PACS numbers: 25.75.Gz,25.75.Ld,12.38.Mh

Typeset using REVTeX

I. INTRODUCTION

The spatio-temporal extension and evolution of the interaction region in heavy-ion collisions are not directly observable. Indirect experimental access to its geometry and dynamics is possible through Hanbury-Brown/Twiss (HBT) intensity interferometry [1,2]. However, the interpretation of the measured HBT correlations is in general model dependent, and the question arises to what extent their interpretational ambiguity can be reduced by an optimal parametrisation and a refined analysis of the data.

In general, HBT radius parameters measure the Gaussian widths (second moments) of the source distribution in space-time [3–7]. It is the finite lifetime of the particle source in heavy ion collisions which complicates their interpretation. For a static boson emitting source, the HBT-radii have a *unique* interpretation in terms of geometrical source sizes. For dynamical sources like those created in heavy ion collisions, however, the HBT-radii measure certain linear combinations of the lifetime, the geometrical sizes and other space-time correlations. This can be clearly seen from the recently derived model-independent expressions for the HBT parameters [3–5,7,8] from which they are also most conveniently calculated in practice. Furthermore, if the source expands all HBT parameters become functions of the pair momentum [9,6].

As long as certain symmetries of the collision region, which exist for vanishing transverse pair momentum, are only weakly broken, four particular second moments of the source contributing to the HBT-radii are generically larger than all the others [5]. Based on this observation the so-called Yano-Koonin-Podgoretskii (YKP) parametrisation [5,10–12] of the correlation function has been advocated recently [5,7]. As we shall review below, one of its main advantages compared to the previously more popular Cartesian one is that three of the four YKP parameters measure as leading terms exactly the three large geometrical (transverse, longitudinal, and temporal) contributions to the HBT-radii, in a particular reference frame (the so-called Yano-Koonin (YK) frame). In contrast to the standard Cartesian parametrisation, this leads, in leading order, to a decoupling of the spatial and temporal

aspects of the source. This facilitates the extraction of the duration of particle emission [7]. The YK-frame in which this decoupling occurs is determined by the Yano-Koonin velocity which itself is one of the four fit parameters. Its dependence on the particle pair momentum provides a direct test for the longitudinal expansion of the source [5,7].

This simple spatio-temporal interpretation of the YKP fit parameters rests on the assumption that, compared to the four leading contributions, all other second space-time moments of the source are small and can be treated systematically as perturbations. So far its validity is supported only by the qualitative arguments of Ref. [5] and by some first numerical checks presented in Ref. [7]. In this paper, we investigate this issue quantitatively through a detailed numerical study of a class of simple models for the emission function, thereby putting the interpretation of the YKP parameters on a firm theoretical foundation. Resonance decays [13,14] are not discussed here but will be deferred to a separate publication [15].

II. HBT FORMALISM

We begin by shortly recalling the basic relations between the emission function $S(x, K)$, the measured two-particle correlation function $C(\mathbf{q}, \mathbf{K})$, and the different Gaussian parametrisations of this correlator in terms of Cartesian or YKP radius parameters. The material presented in this and the following Section is not original, but required for a self-contained presentation of our results in Sec. IV. We start from the relation [16,1,9,17] (here written down for bosons)

$$C(\mathbf{q}, \mathbf{K}) \approx 1 + \frac{|\int d^4x S(x, K) e^{i\mathbf{q} \cdot \mathbf{x}}|^2}{|\int d^4x S(x, K)|^2}. \quad (2.1)$$

The emission function $S(x, p)$ is the (Wigner) phase space density of the boson emitting sources [16,9,17] and denotes the probability that a boson with momentum p is emitted from the space time point x . This Wigner function specifies the one-particle momentum spectrum $P_1(\mathbf{p}) = E_p dN/d^3p = \int d^4x S(x, p)$ as well as the two-particle correlation $C(\mathbf{q}, \mathbf{K})$.

The r.h.s. of (2.1) has to be evaluated at $K = \frac{1}{2}(p_1 + p_2)$ (the average momentum of the particle pair) and $q = p_1 - p_2$ (their corresponding relative momentum) where the p_i are on-shell. Ideally, one would like to “invert” Eq. (2.1) to obtain from the measured 2-particle contribution the complete phase space information $S(x, K)$ about the source. This is, however, not possible in a completely model-independent way. The Fourier transform in (2.1) does not have a unique inverse since the four components of the relative momentum q are not independent, due to the on-shell constraint

$$q^0 = \beta \cdot \mathbf{q}, \quad \beta = \frac{\mathbf{K}}{K_0} \approx \frac{\mathbf{K}}{E_K}, \quad (2.2)$$

which follows from $q \cdot K = 0$. In practice the analysis of HBT correlation data must therefore be based on a comparison with specific models for the emission function $S(x, K)$, with the aim of constraining the class of “reasonable” model sources as far as possible. An important tool for this procedure are the model-independent expressions for the HBT parameters [3,4,8] which allow to calculate from an arbitrary emission function S the characteristic parameters of the two-particle correlation function C by simple quadrature. Experimentally, these HBT parameters are obtained via a multidimensional Gaussian fit to $C(\mathbf{q}, \mathbf{K})$ in momentum space. To compute these Gaussian parameters of the (momentum) correlation function C it is sufficient to use the Gaussian approximation of the (space-time) emission function S ,

$$S(x, K) = N(\mathbf{K}) S(\bar{x}(\mathbf{K}), K) \exp \left[-\frac{1}{2} \tilde{x}^\mu(\mathbf{K}) B_{\mu\nu}(\mathbf{K}) \tilde{x}^\nu(\mathbf{K}) \right] + \delta S(x, K), \quad (2.3)$$

neglecting $\delta S(x, K)$ [6]. Here, the \tilde{x}_μ denote the space-time coordinates relative to the effective “source centre” $\bar{x}(\mathbf{K})$ for pions with momentum \mathbf{K} ,

$$\tilde{x}^\mu(\mathbf{K}) = x^\mu - \bar{x}^\mu(\mathbf{K}), \quad \bar{x}^\mu(\mathbf{K}) = \langle x^\mu \rangle, \quad (2.4)$$

and

$$(B^{-1})_{\mu\nu}(\mathbf{K}) = \langle \tilde{x}_\mu \tilde{x}_\nu \rangle \quad (2.5)$$

is the inverse of the Gaussian curvature tensor in (2.3), adjusted such that the first term in (2.3) reproduces the rms width of the full source $S(x, K)$. The (\mathbf{K} -dependent) expectation values in these definitions are defined as space-time averages over the emission function:

$$\langle f(x) \rangle = \frac{\int d^4x f(x) S(x, K)}{\int d^4x S(x, K)}. \quad (2.6)$$

The correction term δS contains information on the deviation of the emission function $S(x, K)$ from a Gaussian form in coordinate space, i.e. on sharp edges, wiggles, secondary peaks, etc. If the correlator $C(\mathbf{q}, \mathbf{K})$ in momentum space is also parametrised by a Gaussian, such deviations are automatically excluded. We could show numerically, however, that the neglected contributions from δS generally have very little influence on the half width of the correlation function [6], and that the Gaussian approximation for the correlator $C(\mathbf{q}, \mathbf{K})$ remains very good even for sources with strongly non-Gaussian space-time structure. Neglecting δS , the two-particle correlation function $C(\mathbf{q}, \mathbf{K})$ can be calculated analytically from (2.1):

$$C(\mathbf{q}, \mathbf{K}) = 1 + \exp [-q^\mu q^\nu \langle \tilde{x}_\mu \tilde{x}_\nu \rangle(\mathbf{K})]. \quad (2.7)$$

It is fully determined by the \mathbf{K} -dependent second space-time moments $(B^{-1})_{\mu\nu}$ of the source (the “effective widths” $\langle \tilde{x}_\mu \tilde{x}_\nu \rangle(\mathbf{K})$ or “lengths of homogeneity” [4,18]).

A. Gaussian parametrisations of the correlation function

In general, a Gaussian parametrisation of $C(\mathbf{q}, \mathbf{K})$ is specified by selecting a particular choice of three independent components of the relative momentum q and implementing in (2.7) the on-shell constraint $q \cdot K = 0$ accordingly. This is usually done in a Cartesian coordinate system with z along the beam axis and \mathbf{K} lying in the x - z -plane. Customarily one labels the z -component of a 3-vector by l (for *longitudinal*), the x -component by o (for *outward*) and the y -component by s (for *side-ward*). In this coordinate system, the on-shell constraint (2.2) reads

$$q^0 = \beta_\perp q_o + \beta_l q_l \quad (2.8)$$

where $\beta_\perp = |\mathbf{K}_\perp|/K^0 \approx |\mathbf{K}_\perp|/E_K$ denotes (approximately) the velocity of the particle pair transverse to the beam direction, and β_l its longitudinal component.

The standard Cartesian parametrisation [3,4] of the correlation function is obtained by using (2.8) to eliminate q^0 from Eq. (2.7). This determines 6 Cartesian HBT radius parameters R_{ij} in terms of the variances $\langle \tilde{x}_\mu \tilde{x}_\nu \rangle(\mathbf{K})$ of the emission function:

$$C(\mathbf{q}, \mathbf{K}) = 1 + \exp \left[- \sum_{i,j=s,o,l} R_{ij}^2(\mathbf{K}) q_i q_j \right],$$

$$R_{ij}^2(\mathbf{K}) = \langle (\tilde{x}_i - \beta_i \tilde{t})(\tilde{x}_j - \beta_j \tilde{t}) \rangle, \quad i, j = s, o, l. \quad (2.9)$$

For an azimuthally symmetric collision region or an azimuthally symmetric sample of collision events, $C(\mathbf{q}, \mathbf{K})$ is symmetric with respect to $q_s \rightarrow -q_s$ [5]. Then $R_{os}^2 = R_{sl}^2 = 0$ and [3]

$$C(\mathbf{q}, \mathbf{K}) = 1 + \exp \left[-R_s^2(\mathbf{K}) q_s^2 - R_o^2(\mathbf{K}) q_o^2 - R_l^2(\mathbf{K}) q_l^2 - 2R_{ol}^2(\mathbf{K}) q_o q_l \right], \quad (2.10)$$

with [3,8]

$$R_s^2(\mathbf{K}) = \langle \tilde{y}^2 \rangle, \quad (2.11a)$$

$$R_o^2(\mathbf{K}) = \langle (\tilde{x} - \beta_\perp \tilde{t})^2 \rangle, \quad (2.11b)$$

$$R_l^2(\mathbf{K}) = \langle (\tilde{z} - \beta_l \tilde{t})^2 \rangle, \quad (2.11c)$$

$$R_{ol}^2(\mathbf{K}) = \langle (\tilde{x} - \beta_\perp \tilde{t})(\tilde{z} - \beta_l \tilde{t}) \rangle. \quad (2.11d)$$

An alternative way of eliminating the redundant component of q in (2.7) leads to the Yano-Koonin-Podgoretskii parametrisation [5,10,11] of $C(\mathbf{q}, \mathbf{K})$,

$$C(\mathbf{q}, \mathbf{K}) = 1 + \exp \left[-R_\perp^2(\mathbf{K}) q_\perp^2 - R_\parallel^2(\mathbf{K}) (q_l^2 - (q^0)^2) - (R_0^2(\mathbf{K}) + R_\parallel^2(\mathbf{K})) (q \cdot U(\mathbf{K}))^2 \right].$$

$$(2.12)$$

This is based on replacing in Eq. (2.7) q_o and q_s in terms of $q_\perp = \sqrt{q_o^2 + q_s^2}$, q^0 , and q_l . Here, $U(\mathbf{K})$ is a (K -dependent) 4-velocity with only a longitudinal spatial component:

$$U(\mathbf{K}) = \gamma(\mathbf{K}) (1, 0, 0, v(\mathbf{K})), \quad \text{with } \gamma = \frac{1}{\sqrt{1 - v^2}}. \quad (2.13)$$

This parametrisation has the advantage that the YKP parameters $R_\perp^2(\mathbf{K})$, $R_0^2(\mathbf{K})$, and $R_\parallel^2(\mathbf{K})$ extracted from such a fit do not depend on the longitudinal velocity of the observer

system in which the correlation function is measured; they are invariant under longitudinal boosts. The model-independent expressions for these YKP-parameters are most conveniently given in terms of the notational shorthands [7]

$$A = \left\langle \left(\tilde{t} - \frac{\tilde{\xi}}{\beta_{\perp}} \right)^2 \right\rangle, \quad (2.14a)$$

$$B = \left\langle \left(\tilde{z} - \frac{\beta_l}{\beta_{\perp}} \tilde{\xi} \right)^2 \right\rangle, \quad (2.14b)$$

$$C = \left\langle \left(\tilde{t} - \frac{\tilde{\xi}}{\beta_{\perp}} \right) \left(\tilde{z} - \frac{\beta_l}{\beta_{\perp}} \tilde{\xi} \right) \right\rangle, \quad (2.14c)$$

where $\tilde{\xi} \equiv \tilde{x} + i\tilde{y}$ and $\langle \tilde{y} \rangle = \langle \tilde{x}\tilde{y} \rangle = 0$ for azimuthally symmetric sources such that $\langle \tilde{\xi}^2 \rangle = \langle \tilde{x}^2 - \tilde{y}^2 \rangle$. In terms of these expressions one finds [7]

$$v = \frac{A + B}{2C} \left(1 - \sqrt{1 - \left(\frac{2C}{A + B} \right)^2} \right), \quad (2.15a)$$

$$R_{\parallel}^2 = \frac{1}{2} \left(\sqrt{(A + B)^2 - 4C^2} - A + B \right) = B - vC, \quad (2.15b)$$

$$R_0^2 = \frac{1}{2} \left(\sqrt{(A + B)^2 - 4C^2} + A - B \right) = A - vC, \quad (2.15c)$$

$$R_{\perp}^2 = \langle \tilde{y}^2 \rangle. \quad (2.15d)$$

For non-vanishing transverse pair momentum K_{\perp} , the Cartesian (2.9) and the YKP (2.12) parametrisations are equivalent and it is instructive to compare them. The Cartesian parameters can be calculated from the YKP ones via [7]

$$R_{\text{diff}}^2 = R_o^2 - R_s^2 = \beta_{\perp}^2 \gamma^2 \left(R_0^2 + v^2 R_{\parallel}^2 \right), \quad (2.16a)$$

$$R_l^2 = \left(1 - \beta_l^2 \right) R_{\parallel}^2 + \gamma^2 (\beta_l - v)^2 \left(R_0^2 + R_{\parallel}^2 \right), \quad (2.16b)$$

$$R_{ol}^2 = \beta_{\perp} \left(-\beta_l R_{\parallel}^2 + \gamma^2 (\beta_l - v)^2 \left(R_0^2 + R_{\parallel}^2 \right) \right), \quad (2.16c)$$

$$R_s^2 = R_{\perp}^2. \quad (2.16d)$$

There is a slight subtlety for $K_{\perp} = 0$. In this limiting case, the on-shell constraint (2.2) reads $q^0 = \beta_l q_l$ and cannot be used to eliminate in (2.7) q_o and q_s in terms of q_{\perp} , q^0 and q_3 . Hence, strictly speaking, the YKP parametrisation exists only for $K_{\perp} \neq 0$. In practice, however, this does not lead to complications since the $K_{\perp} \rightarrow 0$ limit is well-defined for all YKP-parameters (see Sec. IV B).

B. Space-time interpretation of Gaussian parameters

The relations (2.16) provide a powerful consistency check on the experimental fitting procedure of the correlation radii. They show that both parametrisations contain exactly the same spatio-temporal information. We stress, however, that essential space-time characteristics of the source are more easily extracted from the YKP parameters. This is especially the case for the duration of the particle emission process, the “lifetime” of the source.

To see this, we return to the model-independent expressions (2.11) for the Cartesian HBT radii. These mix spatial and temporal information on the source in a non-trivial way. Their interpretation in various reference systems was extensively discussed by analysing these expressions analytically [3–6] for a large class of (azimuthally symmetric) model emission functions and comparing with the numerically calculated correlation function [6]. An important observation resulting from these studies is that the difference

$$R_{\text{diff}}^2 \equiv R_o^2 - R_s^2 = \beta_{\perp}^2 \langle \tilde{t}^2 \rangle - 2\beta_{\perp} \langle \tilde{x}\tilde{t} \rangle + (\langle \tilde{x}^2 \rangle - \langle \tilde{y}^2 \rangle) \quad (2.17)$$

is generally dominated by the first term on the r.h.s. and thus provides access to the lifetime $\Delta t = \sqrt{\langle t^2 \rangle - \langle t \rangle^2}$ of the source [19]. However, in various model studies (including the present one) the term $\beta_{\perp}^2 \langle \tilde{t}^2 \rangle$ turned out to be much smaller than the terms $\langle \tilde{x}^2 \rangle$ and $\langle \tilde{y}^2 \rangle$ which are the leading contributions to R_o^2 and R_s^2 , respectively [3–6]. As a consequence, the difference of two large terms (with standard statistical error bars) has to be determined very accurately to extract a small contribution; this procedure requires excellent statistics of the data, and this makes the extraction of a small source lifetime from the standard fit difficult [20]. Successful attempts have been reported from low-energy heavy-ion collisions (using 2-proton correlations) where the measured lifetimes are very long: $25 \pm 15 \text{ fm}/c$ in Ar+Sc collisions at $E/A = 80 \text{ MeV}$ [22] and $1400 \pm 300 \text{ fm}/c$ in Xe+Al collisions at $E/A = 31 \text{ MeV}$ [23] (the latter is the typical evaporation time of a compound nucleus). Two-pion correlations at ultra-relativistic energies ($E/A = 200 \text{ GeV}$) so far failed to yield positive evidence for a non-vanishing emission duration [24,25], except for the heaviest collision system Pb+Pb [26], but even there the effective lifetime is only a few fm/c .

Clearly, with a different fit parameter whose leading contribution is $\langle \tilde{t}^2 \rangle$, these problems can be circumvented. The YKP parameter R_0^2 has this important property. To see this we recall [5] that the Yano-Koonin velocity v is zero in the Lorentz frame where the expression (2.14c) for C vanishes. In neighbouring frames where C is small, the Yano-Koonin velocity can be calculated approximately from

$$v \approx \frac{C}{A+B} \approx \frac{\langle \tilde{z}\tilde{t} \rangle}{\langle \tilde{t}^2 \rangle + \langle \tilde{z}^2 \rangle}, \quad (2.18)$$

where in the second approximation we neglected generically small terms [5] proportional to $\langle \tilde{z}\tilde{x} \rangle$, $\langle \tilde{x}\tilde{t} \rangle$, and $\langle \tilde{x}^2 - \tilde{y}^2 \rangle$. In the same limit and frame the expressions for R_0^2 and R_{\parallel}^2 simplify to $R_0^2 \approx A \approx \langle \tilde{t}^2 \rangle$ and $R_{\parallel}^2 \approx B \approx \langle \tilde{z}^2 \rangle$, up to corrections of order v^2 . In the YK frame $v = 0$ we thus have [5,7]

$$R_{\perp}^2(\mathbf{K}) = \langle \tilde{y}^2 \rangle, \quad (2.19a)$$

$$R_{\parallel}^2(\mathbf{K}) = \left\langle \left(\tilde{z} - \frac{\beta_l}{\beta_{\perp}} \tilde{x} \right)^2 \right\rangle - \frac{\beta_l^2}{\beta_{\perp}^2} \langle \tilde{y}^2 \rangle \approx \langle \tilde{z}^2 \rangle, \quad (2.19b)$$

$$R_0^2(\mathbf{K}) = \left\langle \left(\tilde{t} - \frac{1}{\beta_{\perp}} \tilde{x} \right)^2 \right\rangle - \frac{1}{\beta_{\perp}^2} \langle \tilde{y}^2 \rangle \approx \langle \tilde{t}^2 \rangle. \quad (2.19c)$$

In the last two expressions we again dropped the generically small terms mentioned above [5,7]. In Eq. (2.19c) the time duration $\Delta t(\mathbf{K}) = \sqrt{\langle \tilde{t}^2 \rangle}$ during which particles of momentum \mathbf{K} are emitted enters as the leading contribution. In the YKP parametrisation it is fitted directly and not obtained as the difference of two large fit parameters as in the standard fit.

It is instructive to rephrase the main idea of the YKP parametrisation from a more formal viewpoint. For an azimuthally symmetric collision region, the Gaussian approximation (2.3) is determined by 7 effective widths $B_{\mu\nu}(\mathbf{K})$, the 3 terms linear in the side component being zero ($B_{\mu s}(\mathbf{K}) = 0$ for $\mu \neq s$). Due to the on-shell constraint, only four linear combinations (Eqs. (2.11) or (2.15)) of these 7 terms can be extracted from the HBT correlation data. This leads to an intrinsic ambiguity of the spatio-temporal interpretation of these parameters. However, if one selects a Lorentz frame in which the contributions from 3 of the 7 non-vanishing $B_{\mu\nu}$'s are very small and the other 4 are in one-to-one correspondence with the 4 fit parameters, then the spatio-temporal interpretation of the leading contributions of these

fit parameters is straightforward. This is the important feature which the YKP fit has and the Cartesian one has not.

The main purpose of the present paper is to turn the qualitative statement hidden in the approximations in (2.19b,c) into a quantitative one. This requires the use of specific source models. In the following Section we introduce a class of azimuthally symmetric hydrodynamic source models which describe spatially and temporally finite, thermalized particle sources with both transverse and longitudinal expansion. For these models, we then discuss quantitatively to what extent the three terms $\langle \tilde{z}\tilde{x} \rangle$, $\langle \tilde{x}\tilde{t} \rangle$, and $\langle \tilde{x}^2 - \tilde{y}^2 \rangle$ are indeed small compared to the remaining four parameters which characterise the azimuthally symmetric emission function. We can then check how far the intuitive interpretation of the YKP fit parameters according to Eqs. (2.19) holds for physically realistic models.

III. A MODEL FOR A FINITE EXPANDING SOURCE

For our numerical study we have taken the model from Ref. [5] with the emission function

$$S(x, K) = \frac{M_\perp \cosh(\eta - Y)}{(2\pi)^3 \sqrt{2\pi(\Delta\tau)^2}} \exp\left[-\frac{K \cdot u(x)}{T}\right] \exp\left[-\frac{(\tau - \tau_0)^2}{2(\Delta\tau)^2} - \frac{r^2}{2R^2} - \frac{(\eta - \eta_0)^2}{2(\Delta\eta)^2}\right]. \quad (3.1)$$

The first term specifies the shape of the freeze-out hypersurface, the second one is a Lorentz-covariant Boltzmann factor encoding the assumption of local thermal equilibration while the last one has a purely geometrical interpretation. The space-time coordinates in longitudinal and temporal directions are parametrised by the space-time rapidity $\eta = \frac{1}{2} \ln[(t+z)/(t-z)]$ and the longitudinal proper time $\tau = \sqrt{t^2 - z^2}$. In the transverse direction, the radius is $r = \sqrt{x^2 + y^2}$. Accordingly, the measure reads $d^4x = \tau d\tau d\eta r dr d\phi$. The time-component of the pair momentum is set to the on-shell value $K_0 = E_K = \sqrt{m^2 + \mathbf{K}^2}$. This approximation was studied in detail in Ref. [4] where it was shown to be acceptable. Thus the pair momentum K can be parametrised using the momentum rapidity $Y = \frac{1}{2} \ln[(1 + \beta_l)/(1 - \beta_l)]$ and the transverse mass $M_\perp = \sqrt{m^2 + K_\perp^2}$,

$$K^\mu = (M_\perp \cosh Y, K_\perp, 0, M_\perp \sinh Y). \quad (3.2)$$

We implement longitudinal and azimuthally symmetric transverse expansion of the source by parametrising the flow velocity in the form

$$u^\mu(x) = \left(\cosh \eta_l(\tau, \eta) \cosh \eta_t(r), \frac{x}{r} \sinh \eta_t(r), \frac{y}{r} \sinh \eta_t(r), \sinh \eta_l(\tau, \eta) \cosh \eta_t(r) \right). \quad (3.3)$$

For the longitudinal flow rapidity we take $\eta_l(\tau, \eta) = \eta$ independent of τ , i.e. we assume a Bjorken scaling profile [27] $v_l = z/t$ in the longitudinal direction. For the transverse flow rapidity we take a linear profile of strength η_f :

$$\eta_t(r) = \eta_f \left(\frac{r}{R} \right). \quad (3.4)$$

The scalar product in the exponent of the Boltzmann factor can then be written as

$$K \cdot u(x) = M_\perp \cosh(\eta - Y) \cosh \eta_t(r) - K_\perp \frac{x}{r} \sinh \eta_t(r), \quad (3.5)$$

Please note that for non-zero transverse momentum K_\perp , a finite transverse flow breaks the azimuthal symmetry of the emission function via the second term in (3.5). For $\eta_f = 0$ the source has no explicit K_\perp -dependence, and M_\perp is the only relevant scale. As will be discussed in Sec. IV D this gives rise to perfect M_\perp -scaling of the YKP radius parameters in the absence of transverse flow, which is again broken for non-zero transverse flow [28].

Besides η_f , the model parameters are the freeze-out temperature T , the transverse geometric (Gaussian) radius R , the average freeze-out proper time τ_0 as well as the mean proper emission duration $\Delta\tau$, the centre of the source rapidity distribution η_0 , and the (Gaussian) width of the space-time rapidity profile $\Delta\eta$. A rough spatial picture of the source at various fixed coordinate times can be gleaned from the nice Figures 1 and 2 in Ref. [29] (although their source has sharp edges whereas ours is smoothed by Gaussian profiles).

We did our calculations for pions ($m = m_{\pi^\pm} = 139$ MeV/ c^2) and kaons ($m = m_{K^\pm} = 494$ MeV/ c^2).

IV. LIFETIMES AND SIZES FROM THE YKP-FIT TO THE CORRELATION FUNCTION

In this section we present a quantitative study of the YKP fit-parameters, thereby clarifying their physical interpretation. Since the YKP-parameter R_\perp is identical to the “side” radius of the Cartesian parametrisation, $R_\perp^2 = R_s^2 = \langle y^2 \rangle$, its interpretation is obvious and independent of the longitudinal velocity of the reference frame. Hence we focus subsequently on the remaining three parameters R_0^2 , R_\parallel^2 , and v .

Unless stated otherwise, the numerical calculations below are done with the set of source parameters $T = 140$ MeV, $R = 3$ fm, $\Delta\eta = 1.2$, $\tau_0 = 3$ fm/c, $\Delta\tau = 1$ fm/c.

A. The Yano-Koonin velocity

According to Eq (2.13), the YKP-fit parameter v is a longitudinal velocity. In this subsection we give a detailed discussion of the physical interpretation of the reference frame specified by v and establish its relation to several other commonly used reference frames. Their definitions are:

- **CMS**: The centre of mass frame of the fireball, specified by $\eta_0 = 0$.
- **LCMS** (Longitudinally CoMoving System [19]): A pion (kaon) pair-dependent frame, specified by $\beta_l = Y = 0$. In this frame, only the transverse velocity component of the pion (kaon) pair is non-vanishing.
- **LSPS** (Longitudinal Saddle-Point System [30]): The longitudinally moving rest frame of the point of maximal emissivity for a given pair momentum. In general, the velocity of this frame depends on the momentum of the emitted particle pair. For symmetric sources the point of maximal emissivity (“saddle point”) coincides with the “source centre” $\bar{x}(\mathbf{K})$ defined in (2.4). In this approximation, for a source like (3.1), the LSPS velocity is given by the longitudinal component of $u^\mu(\bar{x}(\mathbf{K}))$.

- **YK** (Yano-Koonin frame [7]): The frame for which the YKP velocity parameter vanishes, $v(\mathbf{K}) = 0$. Again, this frame is in general pair momentum dependent.

These four frames are quite different in nature. The velocities (or rapidities) of the CMS and LCMS frames can be easily determined experimentally, the first from the peak in the single particle rapidity distribution, the second from the longitudinal momentum of the measured pion pair. However, the velocity of the LSPS is in a sense more interesting: from its definition it is directly related to the longitudinal expansion velocity of the source which, of course, we would like to know. In fact, longitudinal expansion of the source leads to a characteristic dependence of the LSPS velocity v_{LSPS} on the pair rapidity. This is most easily seen by considering two extreme fireball models:

(1) If the source does not expand, all its elements move with the same velocity (rapidity), namely that of the CMS. Then there is no kinematic difference between different parts of the fireball, and the saddle point is K -independent and given by the peak of the space-time distribution of the source. Thus the rapidity of the LSPS, defined as $Y_{\text{LSPS}} = \frac{1}{2} \ln [(1 + v_{\text{LSPS}})/(1 - v_{\text{LSPS}})]$, is *independent* of the pair rapidity Y and identical to the rapidity of the CMS.

This behaviour of Y_{LSPS} arises automatically if the source has no $x - K$ correlations, i.e. if the emission function factorizes, $S(x, K) = F(x) G(K)$. Then all space-time characteristics of the source, including the LSPS velocity, are determined by $F(x)$ alone and do not depend on K . Hence Y_{LSPS} is independent of Y . Factorization is, however, not necessary for this behaviour: Non-vanishing $x - K$ correlations generated, e.g., by temperature gradients don't induce a Y -dependence of Y_{LSPS} as long as the source does not expand longitudinally.

(2) If we set in Eq. (3.1) $\Delta\eta \rightarrow \infty$, we recover the Bjorken model [27] for a longitudinally infinite source with boost-invariant longitudinal expansion. The only η -dependence then comes from the thermal Boltzmann factor, and the longitudinal saddle point obviously lies at $\eta = Y$. Since for the Bjorken scaling profile η coincides with the longitudinal fluid rapidity, this implies that in this case the rapidity of the LSPS is *identical* with the pair rapidity,

$Y_{\text{LSPS}} = Y$, i.e. the LSPS coincides with the LCMS.

It is obvious from this discussion that knowledge of the function $Y_{\text{LSPS}}(Y)$ would allow to distinguish between these two scenarios: A non-expanding source would yield $Y_{\text{LSPS}}(Y) = \text{const.}$ while a source with boost-invariant longitudinal expansion gives $Y_{\text{LSPS}}(Y) = Y$. Realistic models are expected to lie in between these two extremes.

Unfortunately, the LSPS-velocity $v_{\text{LSPS}}(\mathbf{K})$ cannot be measured. This is clear from its definition as the longitudinal flow velocity evaluated at the point of maximum emissivity. As discussed above, this point is approximately given by the source centre $\bar{x}(\mathbf{K})$ which itself is unmeasurable: it drops out [7] from both the single and two-particle spectra which are invariant under a translation of the source centre (even if \mathbf{K} -dependent!). The only velocity we can measure, namely from an YKP fit of the two-particle correlator, is the Yano-Koonin (YK) velocity $v(\mathbf{K})$ resp. the associated rapidity $Y_{\text{YK}} = \frac{1}{2} \ln [(1+v)/(1-v)]$. It is therefore very gratifying to know that for sufficiently rapidly expanding systems the two velocities are always closely related (although in general not identical). In particular, we will show below that for the class of models (3.1) the function $Y_{\text{YK}}(Y)$ shares with $Y_{\text{LSPS}}(Y)$ the feature that it provides a direct signature for longitudinal expansion.

The close relationship between the (measurable) YK-velocity and the (theoretical) LSPS-velocity for certain source models has been known for years. In Ref. [11] a “symmetric frame” was introduced as the reference frame, in which the production process is symmetric in the beam direction. In this frame, the longitudinal extension and the lifetime of the source reach their extremal values [11]. For moving, but non-expanding azimuthally symmetric sources Podgoretskiĭ found in this way the parametrisation (2.12), with \mathbf{K} -independent parameters R_{\perp} , R_{\parallel} , and R_0 , and with what we call the Yano-Koonin velocity v being identical to the velocity of his “symmetric frame”. In this case the YK-system also coincides with the rest frame of the source as a whole (CMS) as well as with the LSPS.

That the coincidence between the YK and LSPS systems is more generally valid for sources which are symmetric around their saddle point $\bar{x}(\mathbf{K})$ has been observed in Refs. [5,30]. It thus holds for any emission function in the Gaussian saddle-point approxi-

mation, due to the symmetry of the latter. As the following paragraph will show, differences between the YK-velocity and the velocity of the LSPS are only due to asymmetries of the source around its saddle point. Although such asymmetries usually exist for collectively expanding sources with finite geometric extension, they are generally small and can be treated perturbatively. Therefore, the YK-frame and the LSPS-frame are usually very close to each other, $v \approx v_{\text{LSPS}}$. From the examples above it is clear, however, that the same is not true for the LCMS (i.e. the longitudinal rest frame defined by the pair rapidity Y), and that generally $v \neq v_{\text{LCMS}}$.

Let us now discuss the difference $v - v_{\text{LSPS}}$ in more detail. If it is small, so is C when evaluated in the LSPS-frame. From Eqs. (2.18) and (2.14c) we see that then in the LSPS frame v is given by

$$v \approx \frac{C}{A + B} \approx \frac{1}{\langle \tilde{z}^2 \rangle + \langle \tilde{t}^2 \rangle} \left(\langle \tilde{z} \tilde{t} \rangle - \frac{1}{\beta_{\perp}} \langle \tilde{z} \tilde{x} \rangle - \frac{\beta_l}{\beta_{\perp}} \langle \tilde{t} \tilde{x} \rangle + \frac{\beta_l}{\beta_{\perp}^2} \langle \tilde{x}^2 - \tilde{y}^2 \rangle \right), \quad (4.1)$$

where we expanded in first order of the small quantities $\langle \tilde{t} \tilde{x} \rangle, \langle \tilde{z} \tilde{x} \rangle, \langle \tilde{x}^2 - \tilde{y}^2 \rangle$. (The smallness of these terms was argued in [5] and will be checked in the following subsection.) Let us consider the contributions on the r.h.s. term by term. The first and second term reflect the longitudinal asymmetry of the source around the saddle point; they vanish for sources with longitudinal reflection symmetry $\tilde{z} \rightarrow -\tilde{z}$. Similarly, the second and third term vanish unless the reflection symmetry $\tilde{x} \rightarrow -\tilde{x}$ around the saddle point in the “out”-direction is broken (e.g. by transverse flow). A non-zero value of the last term, finally, indicates the breaking of the “out”-“side” rotation symmetry; this can again be caused by transverse source gradients as e.g. transverse flow (see Eq. (3.5)). This proves that the difference $v - v_{\text{LSPS}}$ is entirely due to asymmetries of the source around the saddle point. Furthermore, we will show in Sec. IV B that the last three terms in (4.1) are small for small values of the transverse flow rapidity η_f and/or small values of K_{\perp} . In these limits the difference between v and v_{LSPS} is dominated by the longitudinal source asymmetry, and v is very accurately given by the (leading) first term in (4.1), see Eq. (2.18). Note that in our model the breaking of the longitudinal reflection symmetry is due to the non-symmetric rapidity profile of the

emission function for $Y \neq \eta_0$.

For a quantitative discussion we plot in Fig. 1 the Yano-Koonin rapidity Y_{YK} as well as the difference $Y_{\text{YK}} - Y_{\text{LSPS}}$ as functions of M_{\perp} and Y . All rapidities are given relative to the CMS. One sees that for large values of K_{\perp} the agreement of Y_{YK} with Y_{LSPS} is almost perfect. Also, in this limit both rapidities approach the value of Y , i.e. the YK and LSPS systems coincide with the LCMS. The reason for this is that for large K_{\perp} the Boltzmann term in the emission function (3.1) becomes sharply peaked around the point x where the fluid velocity agrees with the pair velocity; the geometric terms in the emission function are much smoother and can be neglected. The relevant term is the first term in Eq. (3.5), and thus the relevant variable is the transverse mass M_{\perp} . Hence this kinematic region starts for kaons at smaller values of K_{\perp} than for pions (see Fig. 1).

For small values of M_{\perp} , the difference $Y_{\text{YK}} - Y_{\text{LSPS}}$ increases, and both begin to lag behind the LCMS rapidity Y . Still, the YK frame is closer to the LCMS than is the LSPS.

The fact that the YK and LSPS systems track each other so closely implies that the linear rise of the YK rapidity with the pair rapidity Y reflects nothing but a similar rise of the LSPS rapidity with Y . As argued above, the latter is a direct indication for longitudinal expansion of the source. However, it should be noted that this expansion need not necessarily be of hydrodynamic nature. The same feature would be generated by a source consisting of free-streaming pions and resonances which were created at an initial proper time τ_{form} through a boost-invariant production mechanism [27], suffering no further re-scattering. It is easily seen that the strict correlations between coordinates and momenta in a free-streaming gas again lead to a linear dependence of the “source rapidity” Y_{YK} on the pair rapidity, with M_{\perp} -independent unit slope. In fact, it is possible to simulate this situation with the emission function (3.1,3.3) by setting T and η_f to zero, i.e. by eliminating the thermal smearing of the momenta and the transverse collective flow. (Of course, this would also result in vanishing YKP radius parameters, because pions of fixed rapidity Y can come from only a single point in the source.)

A linear rise of Y_{YK} with Y (with approximately unit slope) was recently observed by the GIBS collaboration in Dubna by analysing pion correlations from Mg+Mg collisions at $4.4 A \text{ GeV}/c$. They interpreted their result as evidence for rapid longitudinal expansion of the source. The data were averaged over the transverse pair momentum K_\perp . The data sample was taken with a “central” trigger, but since ^{24}Mg is a rather small nucleus with a large surface to volume ratio it is not clear what fraction of the participating nucleons were stopped to become part of a thermalized fireball. The strong linear increase of Y_{YK} with Y could thus also reflect to some part the free-streaming expansion of the pion sources created in the periphery of the nuclear reaction. Preliminary results of the NA49 collaboration at CERN for Pb+Pb collisions at $158 A \text{ GeV}/c$ also show a rise of Y_{YK} with the pair rapidity Y [26]. Here, however, the Y -dependence of Y_{YK} does not appear to be quite linear, and its slope is less than 1. With all due caution with regard to the still preliminary nature of these results, this may indicate genuine hydrodynamic longitudinal expansion at a somewhat slower rate than resulting from our longitudinal scaling profile. NA49 have also looked separately at a subsample of pairs with $K_\perp > 300 \text{ MeV}/c$, showing that for them the YK rapidity appears to rise more rapidly with Y than in the K_\perp -averaged sample, in agreement with theoretical expectations for a thermalized source (see. Fig. 1a).

The M_\perp -dependence of Y_{YK} can be understood along the same lines. Fig. 1b shows that $Y_{\text{YK}}(Y)$ approximates Y better with increasing transverse mass. In the limit $M_\perp \rightarrow \infty$ the bosons can be emitted only from the source element which moves exactly with the same rapidity, hence $Y_{\text{YK}} \rightarrow Y$. In the opposite limit $M_\perp \rightarrow 0$ the Boltzmann factor in (3.1) becomes a smooth function of x , and the emission function is dominated by the Gaussian geometric terms. In this limit one thus expects the YK rapidity to approach the value $Y_{\text{YK}} = \eta_0$. The numerical results of Fig. 1b show that the value of the pion mass is already large enough for the Boltzmann part of the emission function to become important. As a result the M_\perp -dependence of Y_{YK} is weak in the entire range which can be covered by pions, and even weaker for kaons.

B. Correction terms

In this subsection, we study quantitatively the small correction terms of Eqs. (2.19) and (4.1) which may compromise the approximation (2.18) for v and the simple interpretation of R_{\parallel} and R_0 as longitudinal and temporal widths of the emission function. Since the geometric interpretation of R_{\parallel} and R_0 refers to the YK frame, our analysis will also be done in this frame.

Let us first focus on the central rapidity region $Y = \eta_0$. Then $Y_{\text{YK}} = Y_{\text{LSPS}} = Y$, i.e., the four reference frames listed in Sec. IV A coincide. Furthermore, the source is symmetric in the longitudinal direction and thus $\langle \tilde{x} \tilde{z} \rangle = \langle \tilde{z} \tilde{t} \rangle \equiv 0$. The only non-vanishing corrections thus arise from the terms $\langle \tilde{x} \tilde{t} \rangle$ and $\langle \tilde{x}^2 - \tilde{y}^2 \rangle$. In Fig. 2 they are plotted as a function of K_{\perp} for different values of the scaling parameter η_f for the transverse flow. Without transverse flow (i.e. for $\eta_f = 0$) the source is azimuthally symmetric (see Eq. (3.5)) which implies $\langle \tilde{x}^2 - \tilde{y}^2 \rangle = 0$. Also, the source is reflection symmetric in the out-direction, $\langle \tilde{x} \tilde{t} \rangle = 0$. For non-zero transverse flow the correction terms are generally non-zero, and they grow with increasing η_f . Note that, for fixed η_f and K_{\perp} , the correction terms are considerably smaller for kaons than for pions. This can be understood as follows: as discussed after Eq. (3.5), for $\eta_f = 0$ the source depends only on M_{\perp} , and thus even for non-zero transverse flow everything to zeroth order still scales with M_{\perp} . We will show below that for expanding sources the regions of homogeneity, which effectively contribute to the correlation function, are generically decreasing functions of M_{\perp} . This is thus also true for the correction terms. Since at fixed K_{\perp} the value of M_{\perp} is larger for kaons than for pions, the corresponding correction terms are smaller in absolute terms (although not necessarily relative to the leading contributions).

The K_{\perp} -dependence of the correction terms at non-zero transverse flow $\eta_f \neq 0$ can also be easily understood. The rise of $\langle \tilde{x}^2 - \tilde{y}^2 \rangle$ for increasing transverse momentum is due to the azimuthal symmetry breaking by the second term of Eq. (3.5) which increases both with K_{\perp} and η_f . In contrast, the variance $\langle \tilde{x} \tilde{t} \rangle$ reaches an extremum and then decreases again

for very large K_\perp . This results from an interplay between the increasing breaking of the $\tilde{x} \rightarrow -\tilde{x}$ reflection symmetry, which tends to increase the value for $\langle \tilde{x}\tilde{t} \rangle$, and a decreasing homogeneity length in space-time rapidity η which affects the $t = \tau \cosh \eta$ part of this variance.

In the model independent expressions (2.19) and (4.1) for the YKP parameters, the correction terms discussed above are divided by β_\perp and β_\perp^2 , respectively. From Appendix A we know that the ratios remain finite in the limit $\beta_\perp \rightarrow 0$. Still, the corrections to the YKP parameters could become sizeable, depending on how slowly the variances $\langle \tilde{x}\tilde{t} \rangle$ and $\langle \tilde{x}^2 - \tilde{y}^2 \rangle$ vanish in this limit. In Fig. 2b,d we show that the correction terms actually remain small even after dividing them by the appropriate powers of β_\perp . Thus, at least at mid-rapidity, the leading order approximations (2.19b,c) are seen to be generally very good. The largest correction comes from the difference $\langle \tilde{x}^2 - \tilde{y}^2 \rangle / \beta_\perp^2$ in Eq. (2.19c). A more detailed discussion of its effects on R_0 will follow in the next subsection.

We now proceed to a discussion of the correction terms for $Y \neq \eta_0$. We define $Y_{\text{CM}} = Y - \eta_0$ as the rapidity of the pair in the CMS. In Fig. 3 we compare the correction terms for $Y_{\text{CM}} = 3$ to those for $Y_{\text{CM}} = 0$. Of course, at $Y_{\text{CM}} = 3$ the YK frame no longer coincides with the CMS, see Sec. IV A. Since the transverse variances are not affected by longitudinal boosts nor do they depend on Y (see Appendix A), $\langle \tilde{x}^2 - \tilde{y}^2 \rangle$ does not change with the pair rapidity. However, at a given value of K_\perp the transverse pair velocity $\beta_\perp = K_\perp/E_K$ becomes smaller, since E_K increases with the pair rapidity Y_{CM} . The correction term $\langle \tilde{x}^2 - \tilde{y}^2 \rangle / \beta_\perp^2$ thus increases with Y_{CM} , especially at low K_\perp . A similar effect is seen in the plots for $\langle \tilde{x}\tilde{t} \rangle / \beta_\perp$. While $\langle \tilde{x}\tilde{t} \rangle$ decreases with increasing Y_{CM} , the ratio with β_\perp actually increases by about a factor 2 at small K_\perp . Since in the forward rapidity region the source becomes non-symmetric under reflection $z \rightarrow -z$, $\langle \tilde{x}\tilde{z} \rangle$ and $\langle \tilde{x}\tilde{z} \rangle / \beta_\perp$ are non-zero, but small.

We conclude this subsection with a discussion of the sensitivity of the correction terms to the longitudinal extension of the source, which is parametrised by $\Delta\eta$. We again put $Y_{\text{CM}} = 0$, so that $\langle \tilde{x}\tilde{z} \rangle = 0$. From the explicit expressions given in Appendix A it is clear that the transverse variances $\langle \tilde{x}^2 - \tilde{y}^2 \rangle$ are independent of $\Delta\eta$. Therefore only the size of

$\langle \tilde{x}\tilde{t} \rangle$ changes. In Fig. 4 we show its K_\perp -dependence for different values of $\Delta\eta$. Due to our assumption of freeze-out along a hyperbola of constant proper time τ_0 (smeared by an amount $\Delta\tau$), an increase of $\Delta\eta$ causes a larger effective extension of the source both in the z and in the time direction. This becomes especially important at small K_\perp where the geometrical factors in the emission function (3.1) play an important role. This explains the relatively large $\Delta\eta$ -dependence of $\langle \tilde{x}\tilde{t} \rangle$ at small K_\perp and the weaker dependence at large K_\perp where the source distribution is dominated by the Boltzmann term which does not depend on $\Delta\eta$.

C. Quantitative study of YKP radius parameters

In this subsection we combine the results from the previous subsection for the correction terms with the leading contributions in order to arrive at a quantitative understanding of the longitudinal and temporal YKP radius parameters R_{\parallel} and R_0 , and in particular of their dependence on the pair momentum \mathbf{K} .

In Fig. 5 we show R_0 and R_{\parallel} together with their approximations $\sqrt{\langle \tilde{t}^2 \rangle}$, $\sqrt{\langle \tilde{z}^2 \rangle}$, for pion pairs with rapidity $Y_{\text{CM}} = 0$ and $Y_{\text{CM}} = 3$, respectively, as functions of K_\perp . For vanishing transverse flow both approximations are seen to be exact, in agreement with the discussion from the previous subsection. For non-zero transverse flow the approximation $R_{\parallel} \approx \sqrt{\langle \tilde{z}^2 \rangle}$ remains exact for pairs with $Y_{\text{CM}} = 0$. The reason is that for such pairs the YK rapidity relative to the CMS is zero, and thus the longitudinal velocity β_l (which multiplies the correction terms in (2.19b)) of the pair in the YK frame vanishes. From Fig. 5b one sees, however, that also for forward rapidity pairs at $Y_{\text{CM}} = 3$ the correction terms stay below 10% at all values of K_\perp .

The situation is not quite as good for R_0 . Here one sees apparently strong differences between R_0 and $\sqrt{\langle \tilde{t}^2 \rangle}$ as soon as the transverse flow is switched on. From Fig. 2 it is clear that the correction term $\langle \tilde{x}^2 - \tilde{y}^2 \rangle$ is the culprit and dominates the difference. For a transverse flow of $\eta_f = 0.6$ as shown in Fig. 5a this term becomes (in the experimentally

accessible K_\perp range) larger than $1 \text{ (fm}/c)^2$ and thus comparable to the leading term $\sqrt{\langle \tilde{t}^2 \rangle}$.

From Fig. 5a it may thus appear that R_0 gives really only a rather poor upper estimate for the effective source lifetime $\sqrt{\langle \tilde{t}^2 \rangle}$. However, the numerical results shown in this Figure actually correspond to a rather extreme situation. First, the assumed transverse flow rapidity $\eta_f = 0.6$ is very large, and the heavy ion data at AGS and CERN energies seem to require considerably smaller values [31–33]. Second, the difference between R_0 and $\sqrt{\langle \tilde{t}^2 \rangle}$ is small at low transverse momenta and becomes large only at large K_\perp ; in that range the leading term $\sqrt{\langle \tilde{t}^2 \rangle}$ is essentially given by the source parameter $\Delta\tau$ (see discussion below) which in real experiments [26,29] seems to be larger than the $1 \text{ fm}/c$ assumed here. In realistic situations the relative difference between R_0 and $\sqrt{\langle \tilde{t}^2 \rangle}$ is therefore expected to be much smaller, making R_0 a better estimate for the source lifetime than suggested by Fig. 5. (As an aside, it is noteworthy to realize that, due to the small corrections at low K_\perp , the determination of the source lifetime $\Delta t(\mathbf{K}) = \sqrt{\langle \tilde{t}^2 \rangle}$ from R_0 is particularly clean where its extraction from the standard fit parameters according to $R_{\text{diff}}^2 = R_o^2 - R_s^2 \approx \beta_\perp^2 \langle \tilde{t}^2 \rangle$ becomes difficult due to the β_\perp^2 prefactor. At large K_\perp , the correction terms affect the extraction of Δt from both methods in exactly the same way (see Eqs. (2.17) and (2.19c).)

Fig. 5a shows that the effective source lifetime $\Delta t = \sqrt{\langle \tilde{t}^2 \rangle}$ is a strong function of the pair momentum \mathbf{K} : it is largest at small rapidity Y_{CM} and transverse momentum K_\perp and decreases with increasing Y_{CM} and/or K_\perp . Its asymptotic value for large \mathbf{K} in the CMS is, not unexpectedly, given by the variance (A11) of the proper time distribution of our source (3.1). But why is it larger for pairs with smaller momenta \mathbf{K} ?

We have shortly explained this feature in Ref. [7]: *From Fig. 5b it is clear that the longitudinal region of homogeneity R_{\parallel} is a decreasing function of the pair momentum \mathbf{K} . The reason for this is the same as the similar decrease of R_l in the Cartesian fit and well understood [34] as a consequence of the strong longitudinal expansion of the source. This expansion introduces a longitudinal velocity gradient, and the longitudinal length of homogeneity is given by the inverse of this gradient multiplied by a “thermal smearing factor”*

[4]. The latter reflects the statistical distribution of the particle momenta around the local source fluid velocity, and for a thermal distribution the spatial region over which this thermal smearing is effective decreases with increasing pair momentum. This causes the shrinking of the longitudinal homogeneity length with \mathbf{K} .

Since for different pair momenta R_0 measures the source lifetime in different YK reference frames, the freeze-out “hypersurface” will in general appear to have different shapes for pairs with different momenta. Only in our model, where freeze-out occurs at fixed proper time τ_0 (up to a Gaussian smearing with width $\Delta\tau$), is it frame-independent. It is thus generally unavoidable (and here, of course, true in any frame) that freeze-out at different points z in the source will occur at different times t in the YK frame. Since a z -region of size R_{\parallel} contributes to the correlation function, R_{\parallel} determines how large a domain of this freeze-out surface (and thus how large an interval of freeze-out times in the YK frame) is sampled by the correlator. This interval of freeze-out times combines with the intrinsic Gaussian width $\Delta\tau$ to yield the total effective duration of particle emission. It will be largest at small pair momenta where the homogeneity region R_{\parallel} is biggest, and will reduce to just the variance of the Gaussian proper time distribution at large pair momenta where the longitudinal (and transverse) homogeneity regions shrink to zero. (Since the additional time variance from the shape of the freeze-out surface is largest at small pair momenta, it is again easier to extract from the YKP fit than from the Cartesian one.)

Another interesting feature of Fig. 5 is that at large K_{\perp} both R_{\parallel} and R_0 are independent of the pair rapidity Y . This is a consequence of our boost-invariant longitudinal velocity profile and need not remain true for systems with different longitudinal expansion. As argued before, at large M_{\perp} the space-time shape of the source is dominated by the Boltzmann term and becomes insensitive to the Gaussian geometric factors. The HBT radii thus only see the local velocity gradients which in our case are invariant under longitudinal boosts. At large M_{\perp} pion pairs with different rapidities Y thus all see the same local source structure (remember the identity of the YK and LCMS frames in this limit), and the YKP radii become Y -independent.

We close this subsection with a discussion of the dependence of R_{\parallel} and R_0 on the other source parameters. Since the rapidity dependence does not change qualitatively from what has already been discussed, we concentrate on zero rapidity pion pairs, $Y_{\text{CM}} = 0$. For the transverse flow we choose a non-zero, but more moderate value of $\eta_f = 0.3$.

In Fig. 6 we show the dependence on the longitudinal size of the source which is parametrised by $\Delta\eta$. One sees that at large transverse momenta neither R_{\parallel} nor R_0 and $\sqrt{\langle \tilde{t}^2 \rangle}$ are affected by the with $\Delta\eta$ of the Gaussian geometric factor, in line with the arguments above. At small transverse momenta, both radii increase monotonically with $\Delta\eta$. This means that, at low K_{\perp} , R_{\parallel} becomes sensitive to the global longitudinal geometry of the source and no longer only reflects the local longitudinal velocity gradients. Fig. 6a is very interesting: for small $\Delta\eta$ the longitudinal length of homogeneity is limited by the longitudinal geometry, and R_0 never has a chance to probe a large region of the proper time freeze-out surface. Hence Δt is limited to the variance of the proper time distribution $T(\tau)$ in the source (see (A2,A11)), independent of K_{\perp} . As $\Delta\eta$ increases, at small K_{\perp} the longitudinal length of homogeneity increases too, and R_0 receives an additional contribution from the time variation (in the YK rest frame) along the freeze-out surface inside a longitudinal region of size R_{\parallel} . Thus the rise of the effective source lifetime Δt at small K_{\perp} is an indirect measure for the longitudinal geometric size of the source. Unfortunately, the detailed quantitative dependence is model-dependent.

Fig. 7 shows what happens when the width of the proper time distribution $T(\tau)$ (Eq. (A2)) is changed. Increasing $\Delta\tau$ by 1 fm/ c , R_0 also increases by about 1 fm/ c (slightly less at large K_{\perp} [35]), while R_{\parallel} increases more at small K_{\perp} and less at large K_{\perp} . The increase of R_{\parallel} is due to the decrease of the longitudinal velocity gradient (which for a boost-invariant profile is $1/\tau$) with τ . As the time distribution $T(\tau)$ becomes wider, larger proper times are probed by the emitted pions resulting in larger longitudinal homogeneity regions.

Changing the average freeze-out time τ_0 rather than its spread $\Delta\tau$ has qualitatively similar consequences (see Fig. 8), only that R_0 at sufficiently large K_{\perp} again reduces to the same small variance of the time distribution $T(\tau)$. Please note that, at small K_{\perp} , R_0

increases both with increasing $\Delta\eta$ and increasing $\Delta\tau$; this supports our claim above that it is “sensitive” to the total longitudinal extension of the source $\Delta z \simeq 2\tau_0 \sinh \Delta\eta$. However, the relation is not linear (in particular in our numerical results a doubling of $\Delta\eta$ is seen to have less effect than a doubling of τ_0), making it hard to use in practice. It is obvious that the longitudinal velocity gradient (which decreases by a factor 2 when τ_0 is doubled) has a stronger influence on R_0 and R_{\parallel} than the geometrical width in η .

D. Kaon interferometry, M_{\perp} -scaling, and transverse flow

In this subsection we compare pion and kaon correlation functions. We discuss the M_{\perp} -scaling of the YKP radius parameters and its breaking by transverse collective flow. At the end of the subsection we formulate a program how to extract transverse flow from the M_{\perp} -dependence of the YKP radius parameters.

In Fig. 9 we compare, for central rapidity pairs $Y_{\text{cm}} = 0$, the three YKP radius parameters for pion and kaon pairs, as functions of K_{\perp} . The left column shows a source without transverse expansion, in the right column the transverse flow rapidity was set to $\eta_f = 0.6$. The onset of transverse flow has two qualitative effects: (i) the transverse radius acquires a K_{\perp} -dependence [6], and (ii) R_0 and $\sqrt{\langle \tilde{t}^2 \rangle}$ begin to deviate from each other, as discussed in the previous subsection. (The equality $R_{\parallel}^2 = \langle \tilde{z}^2 \rangle$ remains exact because we are studying pion pairs at $Y_{\text{cm}} = 0$.) The effects of flow on R_{\parallel} and $\sqrt{\langle \tilde{t}^2 \rangle}$ are seen to be weak, for both pions and kaons.

Note also that at small K_{\perp} the kaon radii are generically smaller than the pion radii, with or without transverse flow. This is also seen in experiment [25,36]. However, except for the change in the rest mass we have changed no parameters in the emission function, so the difference must be entirely kinematic. Indeed, it just reflects the fact that for thermalized sources like (3.1) the leading dependence on the particle rest mass is through the variable $M_{\perp} = \sqrt{m^2 + K_{\perp}^2}$. As discussed after Eq. (3.5) the source (3.1) depends *only* on M_{\perp} if it does not expand transversally ($\eta_t(r) = 0$). In this case also the correction terms in Eqs. (2.19b,c)

vanish exactly, and $R_\perp^2 = \langle \tilde{y}^2 \rangle$, $R_\parallel^2 = \langle \tilde{z}^2 \rangle$, and $R_0^2 = \langle \tilde{t}^2 \rangle$ are also functions of M_\perp only. This is shown in the left column of Fig. 10 where the YKP radii for a source without transverse flow are plotted as functions of M_\perp and seen to exactly coincide for pions and kaons in the common M_\perp -range. Since in the absence of transverse flow the Boltzmann factor in (3.1) has no transverse gradients (we have assumed a constant temperature T), the transverse radius R_\perp is M_\perp independent and equal to the transverse geometric (Gaussian) radius R . It was pointed out in Refs. [4,30] that transverse temperature gradients can also cause an M_\perp -dependence of the transverse radius R_\perp ; but since the source remains in this case a function of M_\perp only, the M_\perp -scaling of the YKP radii persists; it can only be broken by transverse flow.

The breaking of the M_\perp -scaling by transverse flow is shown in the right column of Fig. 10, for $\eta_f = 0.6$. It has two origins: the emission function itself is no longer a function of M_\perp only (see (3.5)), and the now non-vanishing correction terms in (2.19b,c) depend on β and thus on both M_\perp and the rest mass m . It is obvious that the scaling violations induced by the pion-kaon mass difference are weak and require very accurate measurements. Furthermore, one may be worried that resonance decay contributions to the correlation radii [13] (which we haven't discussed here) lead also to a breaking of the M_\perp scaling, because they affect pions more than kaons, and this may make it difficult to isolate the transverse flow effects. We will have to postpone a detailed discussion of resonance decays in the context of the model source (3.1) to a future publication [15]. First results [14] indicate, however, that their influence on the M_\perp -dependence of the transverse radius parameter R_\perp is weak. Furthermore, resonances tend to increase all three HBT radii (in particular the effective lifetime R_0), while the M_\perp -scaling violations from transverse flow have the opposite sign for R_\parallel and R_\perp, R_0 .

Detailed dynamical studies of the freeze-out process have shown that the transverse gradients of the temperature across the freeze-out surface tend to be small [37,38]. So the experimentally observed M_\perp -dependence of the transverse radius [24–26] is presumably due

to transverse flow [39]. It was shown in Ref. [6] that the strength of the M_\perp -dependence of R_\perp increases monotonously with the strength η_f of the transverse expansion. Alber [39] has suggested to quantify the strength of collective flow by fitting the HBT radii to a power law in M_\perp ,

$$R_\perp(M_\perp) \propto M_\perp^{-\alpha_\perp}, \quad R_l(M_\perp) \propto M_\perp^{-\alpha_l}, \quad (4.2)$$

and using the magnitude of the extracted (negative) power as a flow measure. He found $\alpha_l \simeq 0.5$ for R_l and smaller values for α_\perp , with a tendency to increase for larger collision systems [39]. He interpreted this as a signature for strong longitudinal and weaker transverse expansion, the latter becoming more important for larger systems.

In Fig. 11 we study the possible conclusions from such an exercise when applied to the results from our model. The left column shows double logarithmic plots for R_\perp and R_\parallel as functions of M_\perp . Obviously the assumption of a power law dependence is well justified for R_\parallel but somewhat marginal for R_\perp . $R_0(M_\perp)$ cannot be approximated by a power law at all. In the right column we show the extracted powers as a function of η_f , the scale parameter for the transverse flow. Since R_\perp is not well represented by a power law, the extracted slope depends somewhat on the fit region, as indicated for the two sets of curves in Fig. 11b. Altogether it is, however, clear that for pions the power α_\perp increases approximately linearly with η_f and for kaons somewhat more strongly. But even for large transverse flow rapidities $\eta_f \simeq 0.5$ the power remains below 0.2. In contrast, the corresponding power α_\parallel in a fit $R_\parallel(M_\perp) \propto M_\perp^{-\alpha_\parallel}$ is already 0.55 in the absence of transverse flow, reflecting the strong boost-invariant longitudinal expansion. (Note that the decrease of R_\parallel with increasing M_\perp is faster than the $\sqrt{T/M_\perp}$ -law suggested in Ref. [34] – see also Ref. [6] for a discussion of this point.) As the transverse flow is switched on, α_\parallel changes much more weakly than α_\perp , showing that R_\parallel is mostly sensitive to the longitudinal flow while R_\perp is only affected by transverse expansion. Again, kaons are affected by the transverse flow more strongly than pions.

V. CONCLUSIONS

We have presented a numerical study of the Yano-Koonin-Podgoretskii fit parameters for the two-particle correlation function. Our starting point were the recently derived model-independent expressions for the YKP parameters in terms of second order space-time variances of the source emission function. These expressions allow for an easy evaluation of the YKP parameters as functions of the pair momentum \mathbf{K} and for detailed parameter studies. We exploited them for a class of hydrodynamic models describing locally thermalized and collectively expanding sources, and we studied the dependence of the YKP parameters on the longitudinal and temporal extension of the source as well as on its longitudinal and transverse expansion velocity.

It has been argued previously that in a certain approximation (which becomes exact in the absence of transverse expansion flow) the YKP parametrisation achieves a perfect factorisation of the longitudinal and transverse spatial and the temporal extensions (“lengths of homogeneity”) of the source, in the comoving frame of the emitting fluid element, and that the velocity of this emitting fluid element is given by the fourth YKP parameter (the YK velocity). Here we have shown numerically that these features are preserved very accurately even in the presence of transverse flow. The transverse radius parameter $R_{\perp}(\mathbf{K})$ gives the effective transverse size of the source, the longitudinal radius parameter $R_{\parallel}(\mathbf{K})$ its effective longitudinal size, both in the local rest frame of the emitter as seen by pairs with momentum \mathbf{K} . More importantly, the YKP parameter $R_0(\mathbf{K})$ provides a direct estimate of the effective emission duration for particles with momentum \mathbf{K} ; this estimate is quite accurate as long as the average transverse flow rapidity remains below 0.5 and the “lifetime parameter” $\Delta\tau$ is not too small ($\Delta\tau > 1 \text{ fm}/c$). The above interpretation is accurate up to small correction terms which we studied extensively in Sec. IV B, both with respect to their magnitude and their \mathbf{K} -dependence. We find that in physically realistic situations they are small enough to be neglected.

We also showed explicitly that the YK velocity obtained from the YKP fit is indeed

approximately equal to the longitudinal velocity of the emitting fluid element (the LSPS velocity), and that the small differences between these two velocities can be understood quantitatively in terms of asymmetries of the source around the point of maximum emissivity (its “saddle point”). This enables us to interpret the rise of the YK rapidity with the pair rapidity Y as a direct consequence of the longitudinal expansion of our source, and the M_\perp -dependence of the slope of the function $Y_{\text{YK}}(Y)$ as a signature for the thermal smearing of the particle momenta in the fluid rest frame. In Ref. [7] we further showed that the slope of the function $Y_{\text{YK}}(Y)$ is nearly independent of the transverse flow rapidity η_f . Thus the YK rapidity is manifestly dominated by the *longitudinal* expansion and hardly affected by the transverse expansion at all. The latter causes, on the other hand, an M_\perp -dependence of the transverse radius parameter R_\perp , which in turn is completely unaffected by the longitudinal expansion. The YKP parametrisation thus not only leads to a factorisation of the (transverse and longitudinal) spatial and temporal aspects of the source *geometry*, but it also cleanly separates its transverse and longitudinal *dynamics*.

The sensitivity of the YKP radius parameters to the transverse expansion of the source was investigated quantitatively in Sec. IV D. While the longitudinal radius parameter R_\parallel is affected very little by the transverse flow (its strong M_\perp -dependence arises from the strong longitudinal flow), the transverse radius shows a considerable dependence on η_f (but none to the longitudinal flow). Furthermore, transverse flow breaks the exact M_\perp -scaling of the YKP radius parameters which we showed to exist for $\eta_f = 0$ [28]. As explained in Sec. IV D, both effects can be combined for a quantitative extraction of the mean transverse expansion velocity from the YKP radius parameters. First results [14] from a comprehensive analysis [15] of resonance decay contributions to the correlation function indicate that they don’t jeopardise such a program.

ACKNOWLEDGMENTS

This work was supported by grants from DAAD, DFG, NSFC, BMBF and GSI. We gratefully acknowledge discussions with H. Appelshäuser, S. Chapman, D. Ferenc, P. Foka, M. Gaździcki, K. Kadija, H. Kalechofsky, P. Seyboth and C. Slotta. U.H. thanks the CERN Theory Group for their warm hospitality.

APPENDIX A: SPACE-TIME MOMENTS OF THE EMISSION FUNCTION

Using cylindrical coordinates τ, η, r, ϕ with $d^4x = \tau d\tau d\eta r dr d\phi$, we can write the emission function (3.1) as

$$S(x, K) d^4x = T(\tau) P(r, \phi) H(r, \eta) d\tau d\eta dr d\phi, \quad (\text{A1})$$

with

$$T(\tau) = \frac{\tau}{\sqrt{2\pi(\Delta\tau)^2}} \exp\left(-\frac{(\tau - \tau_0)^2}{2(\Delta\tau)^2}\right), \quad (\text{A2})$$

$$P(r, \phi) = \frac{1}{2\pi} e^{b(r) \cos \phi}, \quad (\text{A3})$$

$$H(r, \eta) = \frac{r}{(2\pi)^2} \exp\left(-\frac{r^2}{2R^2} - \frac{(\eta - \eta_0)^2}{2(\Delta\eta)^2}\right) M_\perp \cosh(\eta - Y) e^{-a(r) \cosh(\eta - Y)}, \quad (\text{A4})$$

where we defined

$$a(r) = \frac{M_\perp}{T} \cosh \eta_t(r), \quad (\text{A5})$$

$$b(r) = \frac{K_\perp}{T} \sinh \eta_t(r). \quad (\text{A6})$$

The ϕ and τ integrations can be done analytically. We use

$$\int_0^{2\pi} \frac{d\phi}{2\pi} e^{b \cos \phi} \cos(n\phi) = I_n(b) \quad (\text{A7})$$

and define

$$T_0 = \langle 1 \rangle_\tau = \int_{-\infty}^{\infty} T(\tau) d\tau = \tau_0, \quad (\text{A8})$$

$$T_1 = \langle \tau \rangle_\tau = \int_{-\infty}^{\infty} \tau T(\tau) d\tau = \tau_0^2 + (\Delta\tau)^2, \quad (\text{A9})$$

$$T_2 = \langle \tau^2 \rangle_\tau = \int_{-\infty}^{\infty} \tau^2 T(\tau) d\tau = \tau_0^3 + 3\tau_0(\Delta\tau)^2. \quad (\text{A10})$$

The variance of the τ -distribution $T(\tau)$ is

$$\langle \tau^2 \rangle_\tau - \langle \tau \rangle_\tau^2 = (\Delta\tau)^2 \left(1 - \left(\frac{\Delta\tau}{\tau_0} \right)^2 \right). \quad (\text{A11})$$

Defining further

$$\langle f(r, \eta) \rangle_* = \frac{\int_0^\infty dr \int_{-\infty}^\infty d\eta H(r, \eta) I_0(b(r)) f(r, \eta)}{\int_0^\infty dr \int_{-\infty}^\infty d\eta H(r, \eta) I_0(b(r))} \quad (\text{A12})$$

we find for the non-vanishing moments up to second order

$$\langle x^2 \rangle = \frac{1}{2} \left\langle r^2 \left(1 + \frac{I_2(b(r))}{I_0(b(r))} \right) \right\rangle_*, \quad (\text{A13})$$

$$\langle y^2 \rangle = \frac{1}{2} \left\langle r^2 \left(1 - \frac{I_2(b(r))}{I_0(b(r))} \right) \right\rangle_*, \quad (\text{A14})$$

$$\langle z^2 \rangle = \frac{T_2}{T_0} \left\langle \sinh^2 \eta \right\rangle_*, \quad (\text{A15})$$

$$\langle t^2 \rangle = \frac{T_2}{T_0} \left\langle \cosh^2 \eta \right\rangle_*, \quad (\text{A16})$$

$$\langle x \rangle = \left\langle r \frac{I_1(b(r))}{I_0(b(r))} \right\rangle_*, \quad (\text{A17})$$

$$\langle z \rangle = \frac{T_1}{T_0} \langle \sinh \eta \rangle_*, \quad (\text{A18})$$

$$\langle t \rangle = \frac{T_1}{T_0} \langle \cosh \eta \rangle_*, \quad (\text{A19})$$

$$\langle xt \rangle = \frac{T_1}{T_0} \left\langle r \cosh \eta \frac{I_1(b(r))}{I_0(b(r))} \right\rangle_*, \quad (\text{A20})$$

$$\langle zt \rangle = \frac{T_2}{T_0} \langle \sinh \eta \cosh \eta \rangle_*, \quad (\text{A21})$$

$$\langle xz \rangle = \frac{T_1}{T_0} \left\langle r \sinh \eta \frac{I_1(b(r))}{I_0(b(r))} \right\rangle_*. \quad (\text{A22})$$

For $\eta_f \neq 0$ the $\langle \dots \rangle_*$ -averages have to be done numerically. For convenience we also give

$$\langle \tilde{x}t \rangle = \frac{T_1}{T_0} \left[\left\langle r \cosh \eta \frac{I_1(b(r))}{I_0(b(r))} \right\rangle_* - \left\langle r \frac{I_1(b(r))}{I_0(b(r))} \right\rangle_* \langle \cosh \eta \rangle_* \right], \quad (\text{A23})$$

$$\langle \tilde{x}^2 - \tilde{y}^2 \rangle = \left\langle r^2 \frac{I_2(b(r))}{I_0(b(r))} \right\rangle_* - \left\langle r \frac{I_1(b(r))}{I_0(b(r))} \right\rangle_*^2. \quad (\text{A24})$$

Please note that for small arguments $I_n(b) \sim b^n$. Thus for small η_f and/or K_\perp , $\langle \tilde{x}t \rangle$ and $\langle \tilde{x}^2 - \tilde{y}^2 \rangle$ vanish linearly and quadratically, respectively.

REFERENCES

* On leave of absence from Institute of Particle Physics, Hua-Zhong Normal University, Wuhan, China.

- [1] M. Gyulassy, S.K. Kauffmann, and L.W. Wilson, Phys. Rev. **C20**, 2267 (1979).
- [2] D. Boal, C.K. Gelbke and B. Jennings, Rev. Mod. Phys. **62**, 553 (1990).
- [3] S. Chapman, P. Scotto, and U. Heinz, Phys. Rev. Lett. **74**, 4400 (1995).
- [4] S. Chapman, P. Scotto, and U. Heinz, Heavy Ion Physics **1**, 1 (1995).
- [5] S. Chapman, J.R. Nix, and U. Heinz, Phys. Rev. **C52**, 2694 (1995).
- [6] U.A. Wiedemann, P. Scotto and U. Heinz, Phys. Rev. **C53**, 918 (1996).
- [7] U. Heinz, B. Tomášik, U.A. Wiedemann, and Y.-F. Wu, Phys. Lett. B, in press ⟨nucl-th/9603011⟩.
- [8] M. Herrmann and G.F. Bertsch, Phys. Rev. **C51**, 328 (1995).
- [9] S. Pratt, Phys. Rev. Lett. **53**, 1219 (1984); Phys. Rev. **D33**, 1314 (1986).
- [10] F. Yano and S. Koonin, Phys. Lett. **78B**, 556 (1978).
- [11] M.I. Podgoretskiĭ, Sov. J. Nucl. Phys. **37**, 272 (1983).
- [12] GIBS Coll., M.Kh. Anikina et al., Dubna preprint JINR E1-95-311 (1995), submitted to Phys. Lett. B.
- [13] B.R. Schlei, U. Ornik, M. Plümer, and R. Weiner, Phys. Lett. **B293**, 275 (1992); J. Bolz, U. Ornik, M. Plümer, B.R. Schlei, and R. Weiner, Phys. Lett. **B300**, 404 (1993); and Phys. Rev. **D47**, 3860 (1993).
- [14] U. Heinz, in *Quark Matter '96*, (Ref. [26]); U.A. Wiedemann, *ibid.* (poster).
- [15] U.A. Wiedemann and U. Heinz, *Resonance decay contributions to HBT correlation radii*,

Regensburg preprint TPR-96-14, unpublished.

- [16] E. Shuryak, Phys. Lett. **B44**, 387 (1973); Sov. J. Nucl. Phys. **18**, 667 (1974).
- [17] S. Chapman and U. Heinz, Phys. Lett. **B340**, 250 (1994).
- [18] S.V. Akkelin and Y.M. Sinyukov, Phys. Lett. **B356**, 525 (1995).
- [19] T. Csörgő and S. Pratt, in *Proceedings of the Workshop on Relativistic Heavy Ion Physics at Present and Future Accelerators*, Budapest, 1991, edited by T. Csörgő et al. (MTA KFKI Press, Budapest, 1991), p. 75.
- [20] The situation may be better for very long-lived sources which are predicted by hydrodynamics if there is a phase transition to a quark-gluon plasma and the collision fireball is initiated within a certain range of energy densities [21].
- [21] D.H. Rischke and M. Gyulassy, Columbia preprint CU-TP-756 ⟨nucl-th/9606039⟩.
- [22] M.A. Lisa et al., Phys. Rev. Lett. **71**, 2863 (1993).
- [23] M.A. Lisa et al., Phys. Rev. **C49**, 2788 (1994).
- [24] NA35 Coll., T. Alber et al., Z. Phys. **C66**, 77 (1995);
NA35 Coll., T. Alber et al., Phys. Rev. Lett. **74**, 1303 (1995).
- [25] NA44 Coll., H. Beker et al., Phys. Rev. Lett. **74**, 3340 (1995).
- [26] K. Kadija for the NA49 Coll., in *Quark Matter '96*, (Heidelberg, 20.-24.5.1996), edited by P. Braun-Munzinger et al., Nucl. Phys. A, in press.
- [27] J.D. Bjorken, Phys. Rev. **D27**, 140 (1983).
- [28] U. Heinz, B. Tomášik, U.A. Wiedemann, and Y.-F. Wu, Heavy Ion Physics (1996), in press ⟨nucl-th/9606041⟩.
- [29] S. Chapman and J.R. Nix, Phys. Rev. C, in press ⟨nucl-th/9603007⟩.

[30] T. Csörgő and B. Lörrstad, Lund University preprint LUNFD6/(NFFL-7082) ⟨hep-ph/9509213⟩; and Nucl. Phys. **A590**, 465c (1995).

[31] K.S. Lee, U. Heinz, and E. Schnedermann, Z. Phys. **C48**, 525 (1990); E. Schnedermann and U. Heinz, Phys. Rev. Lett. **69**, 2908 (1992); E. Schnedermann, J. Sollfrank, and U. Heinz, Phys. Rev. **C48**, 2462 (1993).

[32] P. Braun-Munzinger, J. Stachel, J.P. Wessels, and N. Xu, Phys. Lett. **B344**, 43 (1994); J. Stachel, in *Quark Matter '96* (Ref. [26]).

[33] N. Herrmann, in *Quark Matter '96*, (Ref. [26]).

[34] A.N. Makhlin and Yu.M. Sinyukov, Z. Phys. **C39**, 69 (1988).

[35] Actually, the proper way of looking at this increase is by studying the variance of the function $T(\tau)$: according to Eq. (A11) it increases from $0.89 \text{ fm}/c$ for $\Delta\tau = 1 \text{ fm}/c$ to $1.49 \text{ fm}/c$ for $\Delta\tau = 2 \text{ fm}/c$.

[36] E802 Coll., V. Cianciolo et al., Nucl. Phys. **A590**, 459c (1995).

[37] U. Heinz, K.S. Lee, and E. Schnedermann, in *The Nuclear Equation of State*, edited by W. Greiner and H. Stöcker, NATO ASI Series 216B, p. 385 (Plenum, New York, 1990).

[38] U. Mayer, PhD thesis, University of Regensburg, 1995, unpublished.

[39] NA49 Coll., T. Alber et al., Nucl. Phys. **A590**, 453c (1995); T. Alber, PhD thesis, MPI für Physik, München (1995), unpublished.

FIGURES

FIG. 1. (a) The rapidity of the YK frame as a function of the pair rapidity Y (both measured in the source CMS), for pions (solid) and kaons (dashed) and for transverse momenta $K_\perp = 1$ MeV and $K_\perp = 1000$ MeV. The transverse flow was set to $\eta_f = 0.3$. (b) Same as (a), but shown as a function of M_\perp for different values of Y . (c) The difference $Y_{\text{YK}} - Y_{\text{LSPS}}$ (see text), plotted in the same way as (a). (d) Same as (c), but shown as a function of M_\perp for different values of Y .

FIG. 2. The correction terms $\langle \tilde{x}^2 - \tilde{y}^2 \rangle$ (a) and $\langle \tilde{x}\tilde{t} \rangle$ (c), for pairs with $Y = 0$ in the CMS, as functions of K_\perp for different values of η_f . The third correction term $\langle \tilde{x}\tilde{z} \rangle$ vanishes at $Y = 0$. Solid (dashed) lines refer to pion (kaon) pairs. Figures (b) and (d) show the same quantities, but scaled by the appropriate inverse powers of β_\perp (see text).

FIG. 3. Same as Fig. 2, but now for a fixed transverse flow $\eta_f = 0.3$ and pions only, but for two different pair rapidities, $Y_{\text{CM}} = 0$ (solid) and $Y_{\text{CM}} = 3$ (dashed).

FIG. 4. Dependence of the correction term $\langle \tilde{x}\tilde{t} \rangle(K_\perp)$ on the longitudinal width parameter $\Delta\eta$, for pion pairs with $Y_{\text{CM}} = 0$.

FIG. 5. (a) R_0 and $\sqrt{\langle \tilde{t}^2 \rangle}$ as functions of K_\perp for $\eta_f = 0$ and $\eta_f = 0.6$, for pion pairs with rapidity $Y_{\text{CM}} = 0$ and $Y_{\text{CM}} = 3$. The lifetime $\sqrt{\langle \tilde{t}^2 \rangle}$ is evaluated in the YK rest frame. (b) Same as (a), but for R_{\parallel} and the longitudinal length of homogeneity $\sqrt{\langle \tilde{z}^2 \rangle}$ in the YK rest frame. For $Y_{\text{CM}} = 0$, R_{\parallel} and $\sqrt{\langle \tilde{z}^2 \rangle}$ agree exactly because $\beta_l = 0$ in the YK frame.

FIG. 6. (a) R_0 and $\sqrt{\langle \tilde{t}^2 \rangle}$ as functions of K_\perp , for different longitudinal gaussian widths $\Delta\eta$. The diagrams are for pion pairs with $Y_{\text{CM}} = 0$ and for transverse flow $\eta_f = 0.3$. The lifetime $\sqrt{\langle \tilde{t}^2 \rangle}$ is evaluated in the YK rest frame which coincides here with the CMS and the LCMS. (b) Same as (a), but for R_{\parallel} . Since $Y_{\text{CM}} = 0$, R_{\parallel} and the longitudinal length of homogeneity in the YK frame $\sqrt{\langle \tilde{z}^2 \rangle}$ agree exactly.

FIG. 7. Same as Fig. 6, but for different widths $\Delta\tau$ of the proper time distribution in the source.

FIG. 8. Same as Fig. 6, but for different average freeze-out times τ_0 .

FIG. 9. The YKP radii R_\perp (top row), R_\parallel (middle row), and R_0 (bottom row), for $Y_{\text{CM}} = 0$ pion (solid) and kaon (dashed) pairs, as functions of K_\perp . Left column: no transverse flow. Right column: transverse flow $\eta_f = 0.6$. In the lower right panel we also show the effective lifetime in the YK frame $\sqrt{\langle \tilde{t}^2 \rangle}$ for comparison. For more discussion see text.

FIG. 10. Same as Fig. 9, but plotted as functions of M_\perp .

FIG. 11. (a) R_\perp as a function of M_\perp at $Y_{\text{CM}} = 0$, for pions (solid) and kaons (dashed) and different transverse flow rapidities η_f . (b) The scaling coefficient α_\perp defined by $R_\perp \approx M_\perp^{-\alpha_\perp}$ for pions (solid) and kaons (dashed) as a function of the transverse flow rapidity η_f . The different results obtained by fitting in the regions $M_\perp - m < 500 \text{ MeV}/c^2$ and $M_\perp - m < 1000 \text{ MeV}/c^2$ are shown separately. (c) Same as (a), but for R_\parallel . (d) Same as (b), but for α_\parallel .

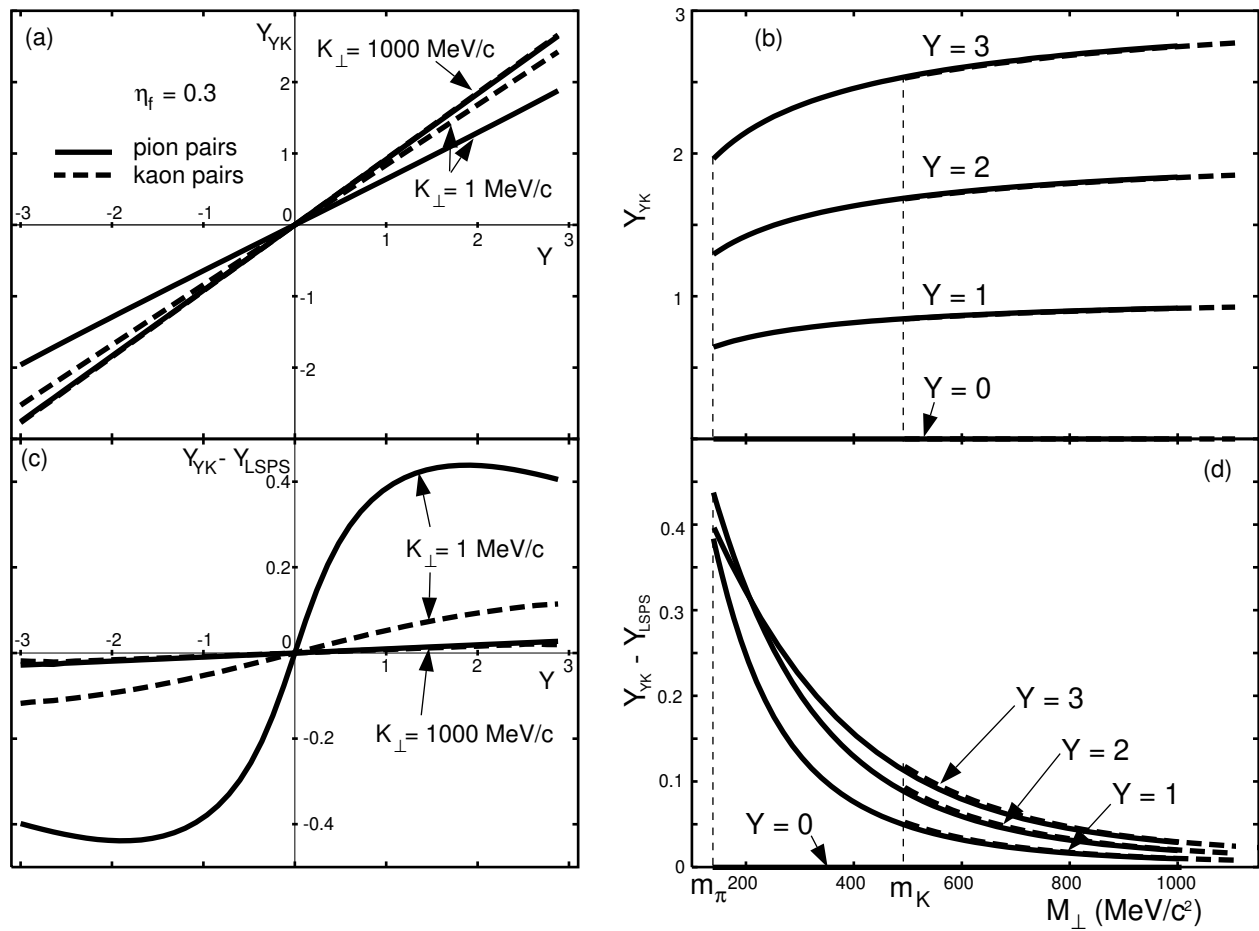


Fig.1

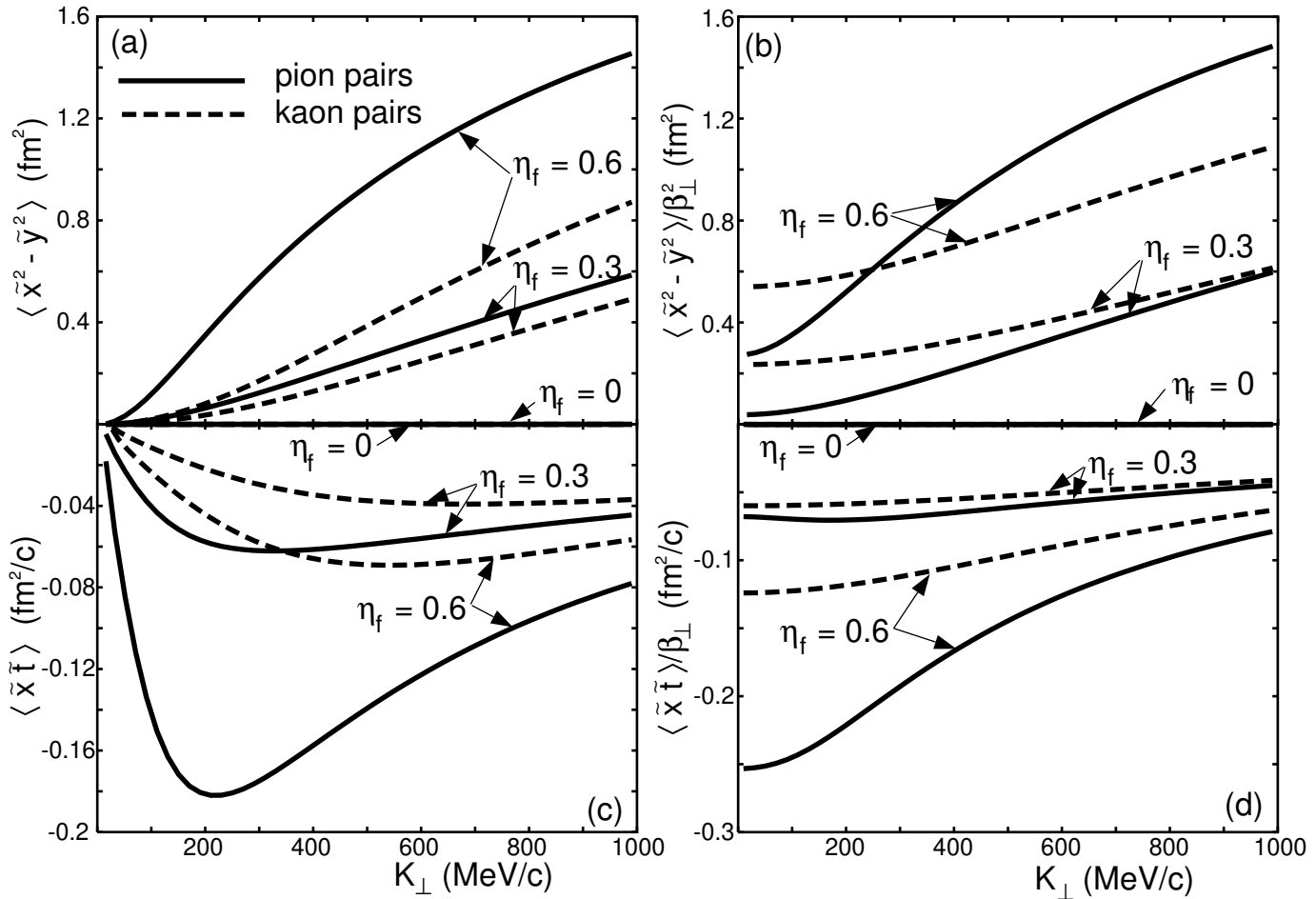


Fig.2

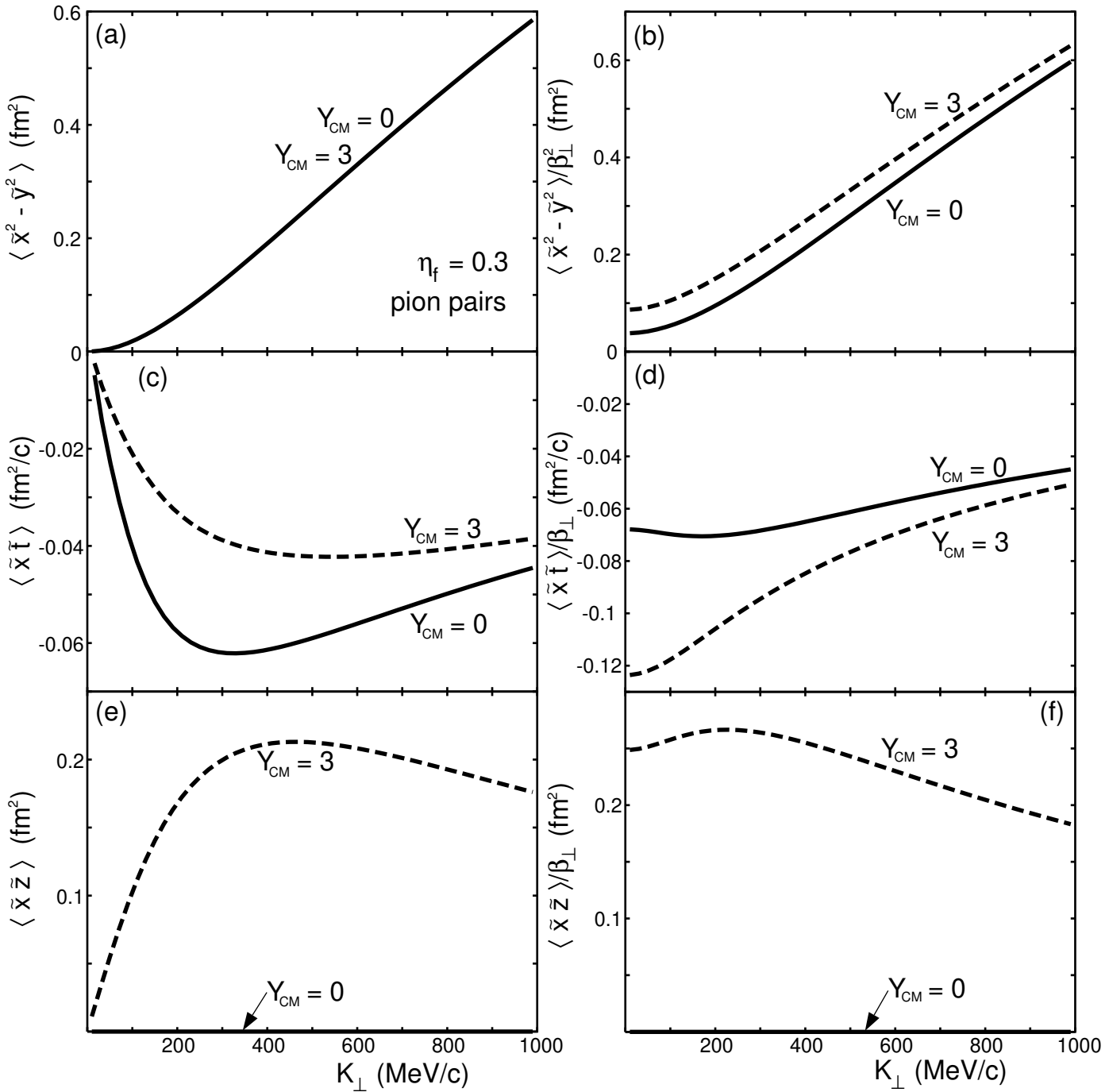


Fig.3

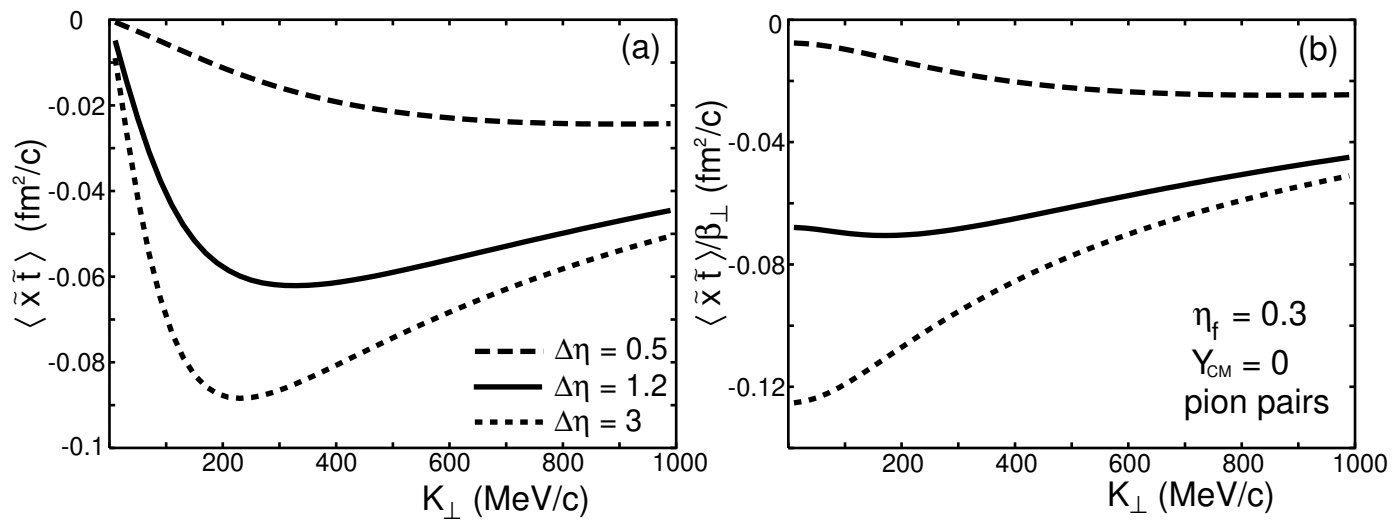


Fig.4

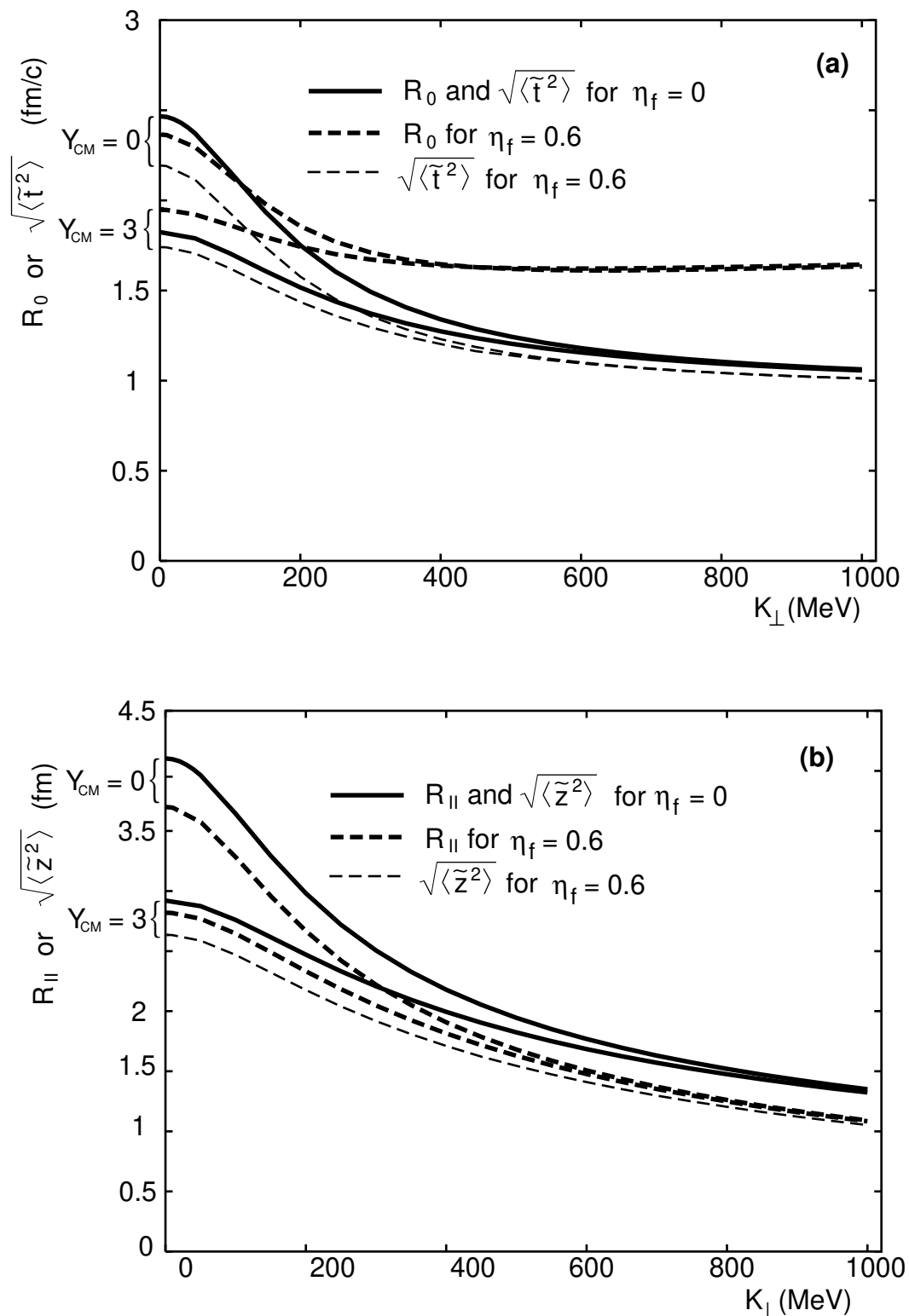


Fig.5

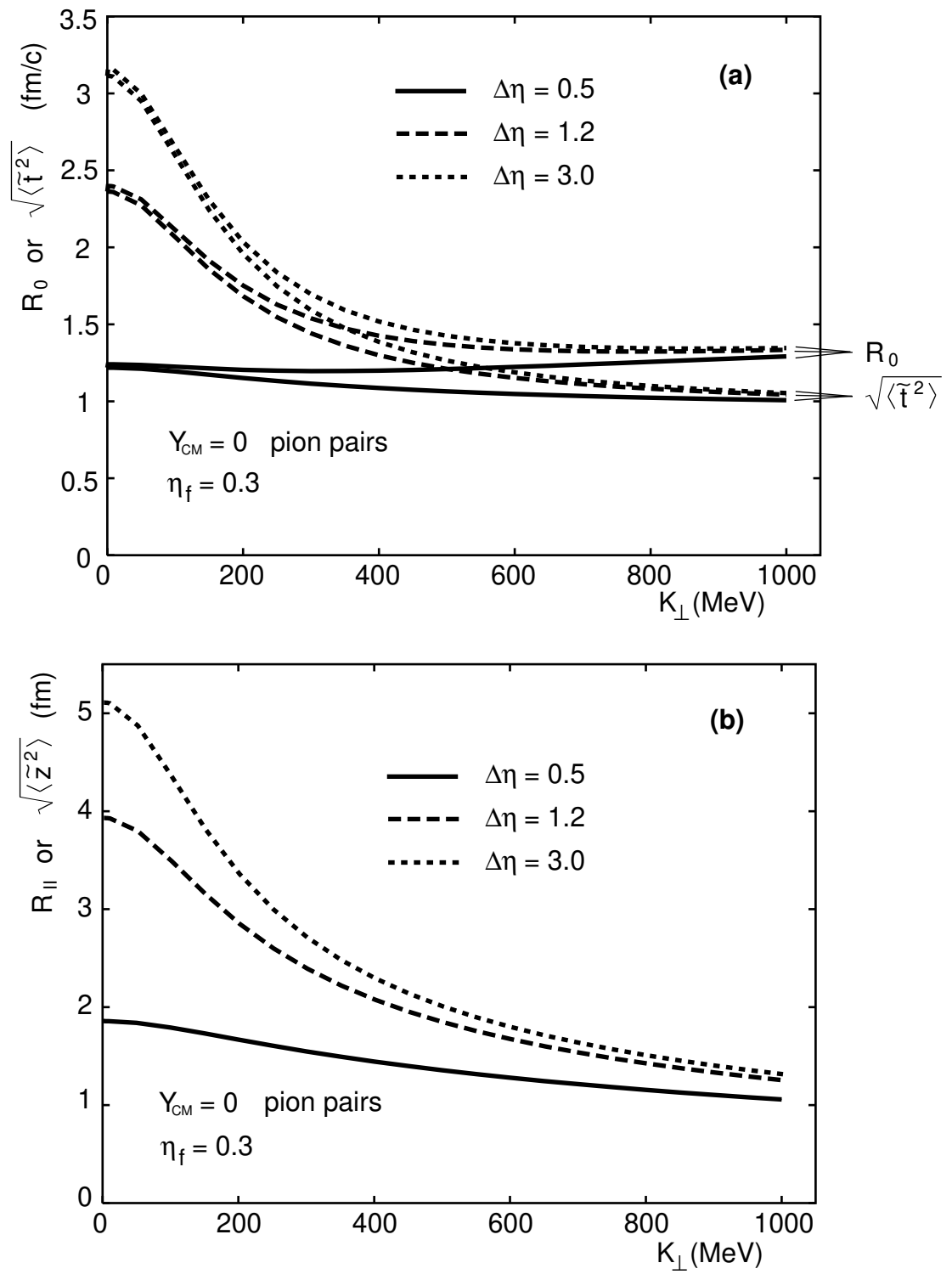


Fig.6

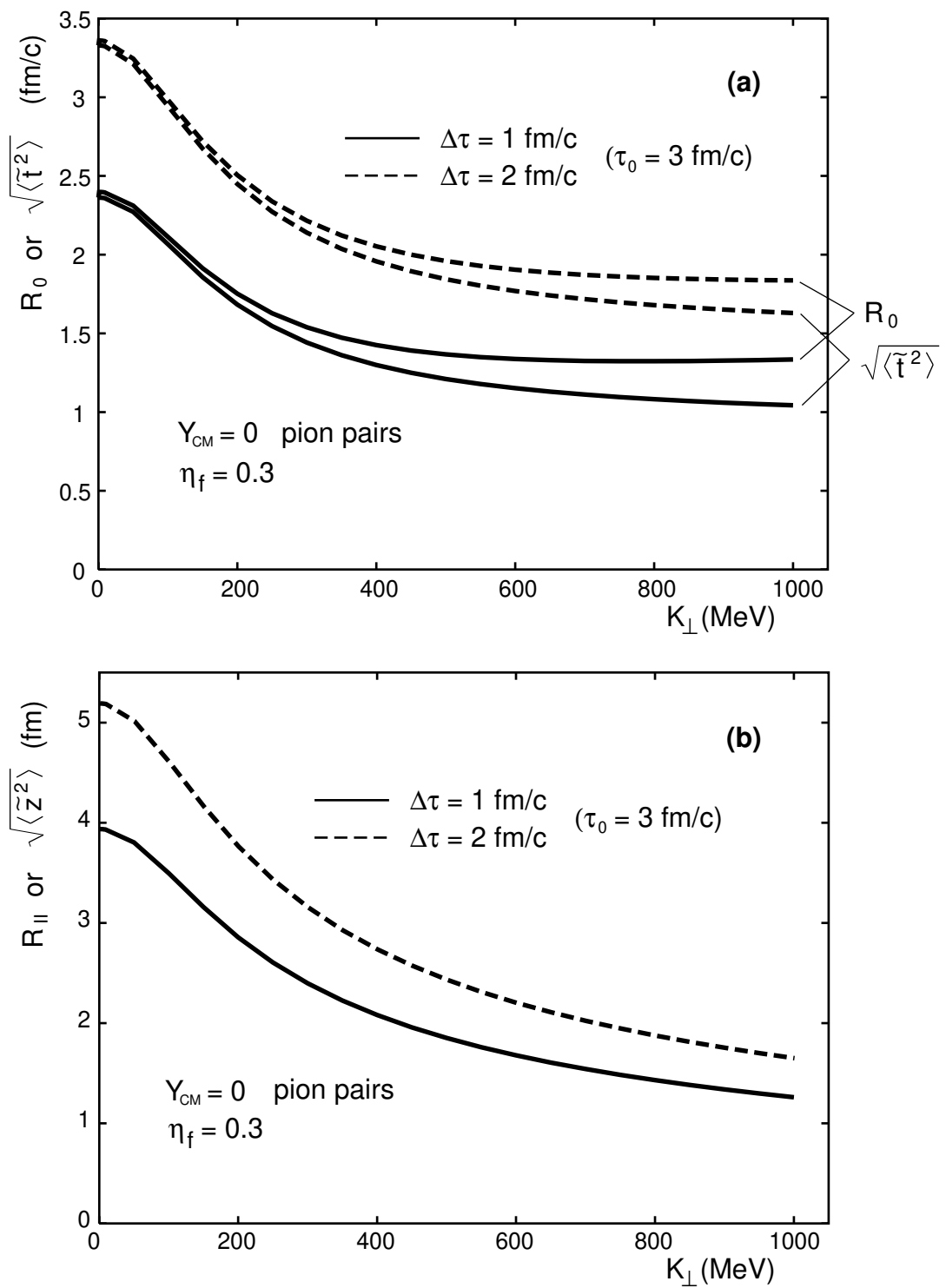


Fig.7

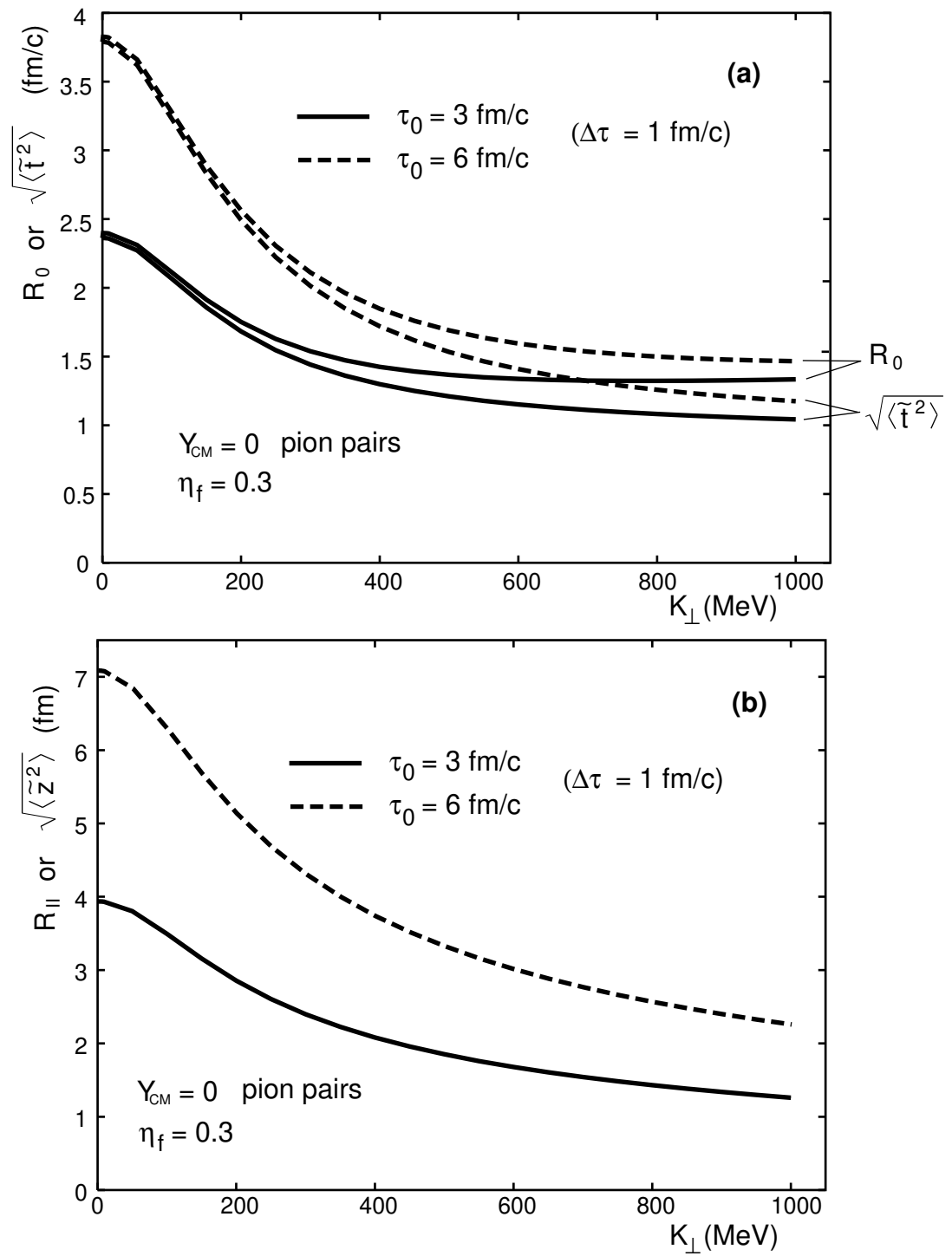


Fig.8

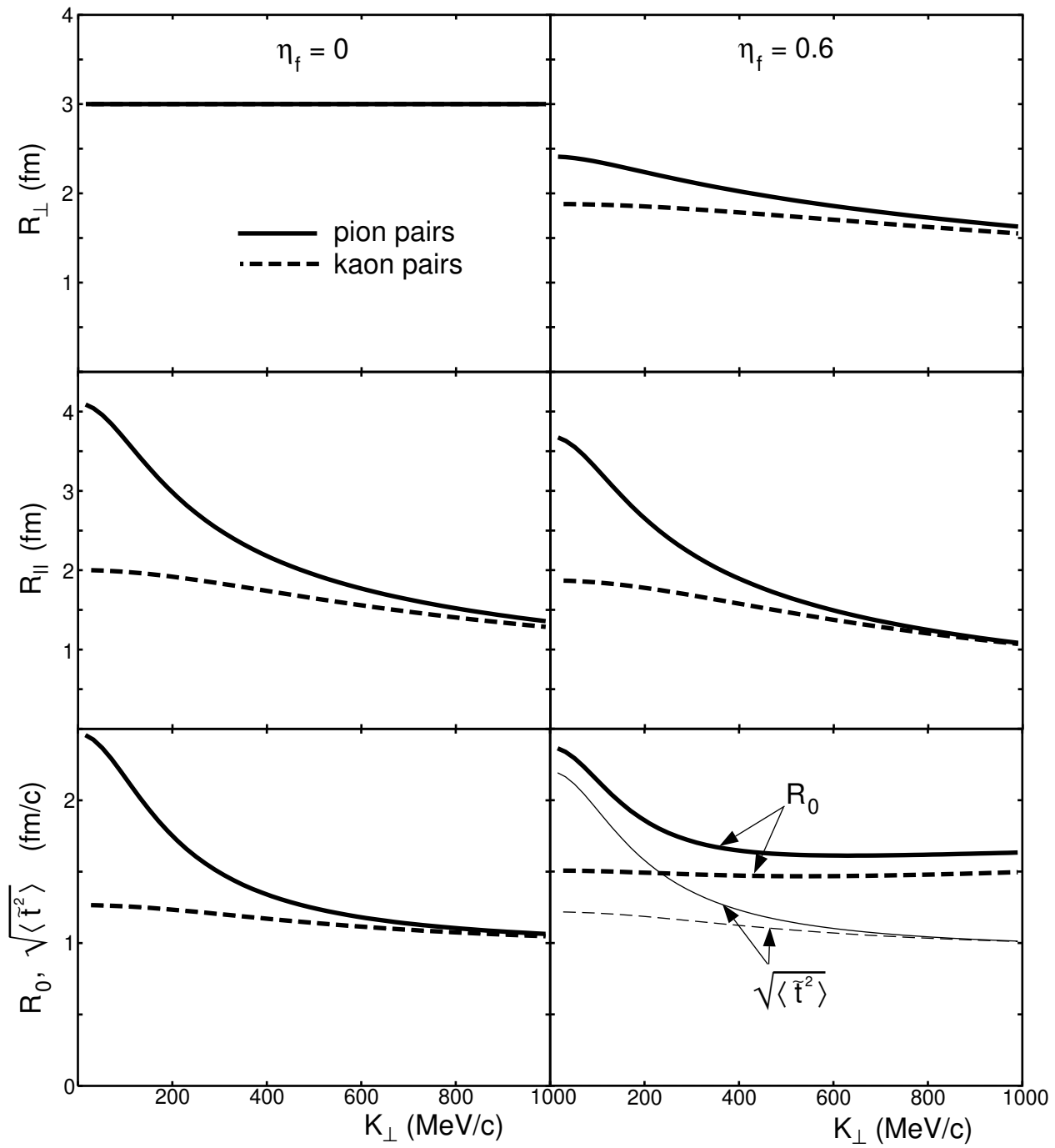


Fig.9

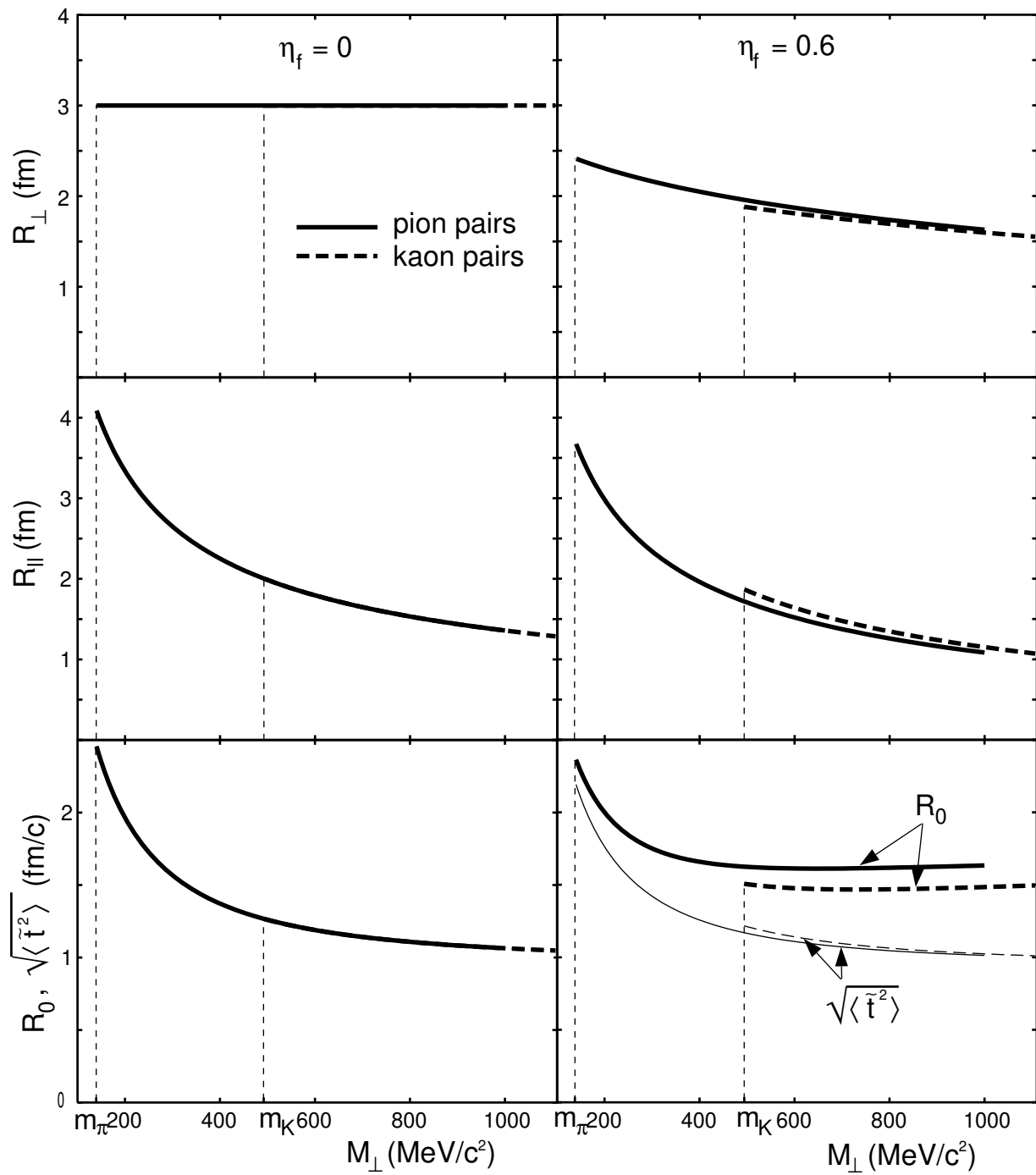


Fig.10

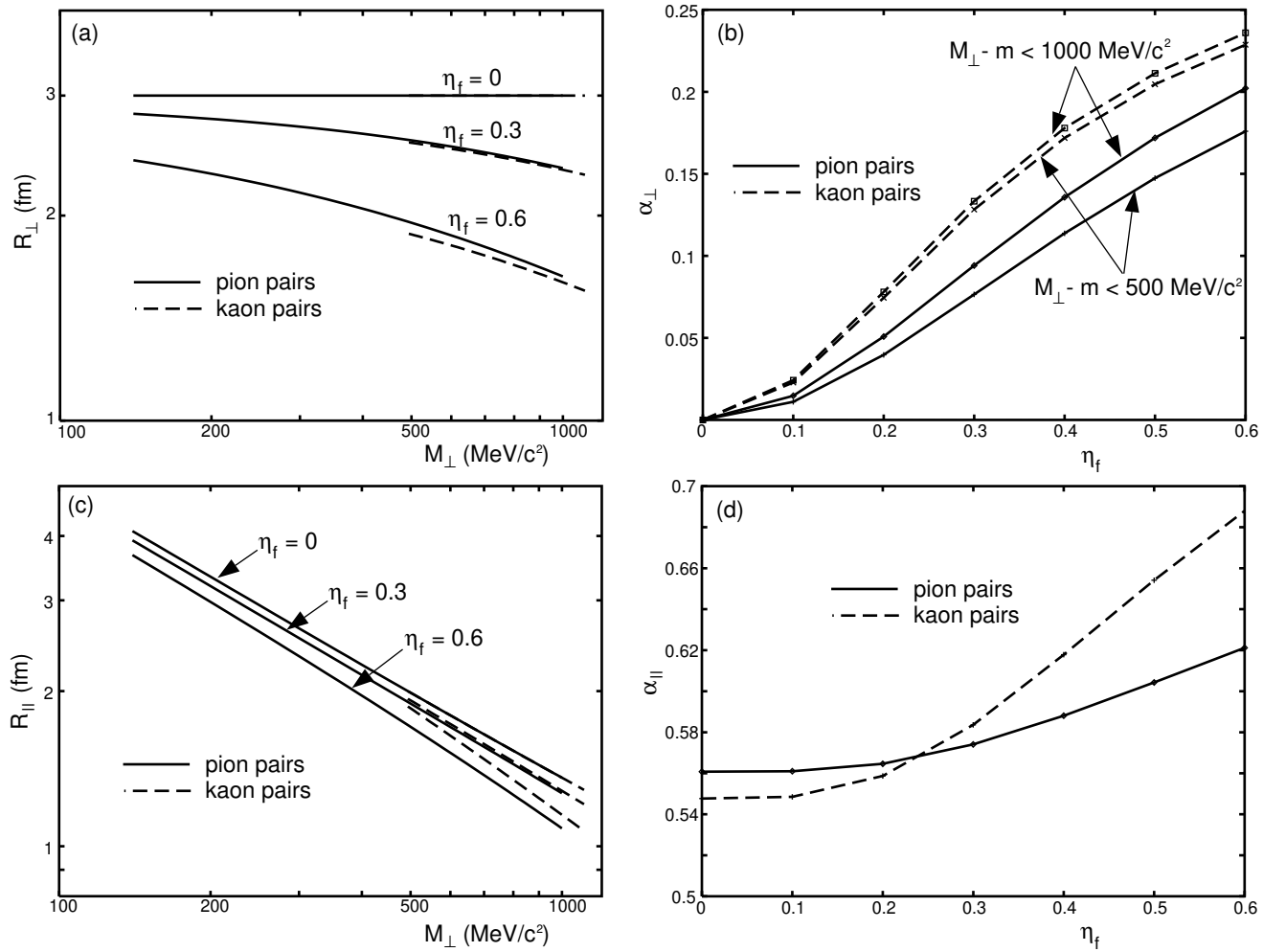


Fig.11

